Available online at www.sciencedirect.com
SCIENCE DIRECT®
Precambrian Research 134 (2004) 113–141
Precambrian Research
www.elsevier.com/locate/precamres

Neoarchaean volcanic rocks, Central Hearne supracrustal belt, Western Churchill Province, Canada: geochemical and isotopic evidence supporting intra-oceanic, supra-subduction zone extension

H.A. Sandeman*, S. Hanmer, W.J. Davis, J.J. Ryan, T.D. Peterson

Geological Survey of Canada, 601 Booth St., Ottawa, Ont., Canada K1A 0E8

Received 18 June 2003; accepted 27 March 2004

Abstract

The Kaminak segment of the Central Hearne supracrustal belt (CHSB) Western Churchill Province, Canada, comprises a diverse sequence of Neoarchaean volcanic and less abundant metasedimentary rocks that were emplaced as two assemblages between 2695–2711 Ma and 2681–2686 Ma, respectively. These are intruded by uncommon pre-tectonic diorites and tonalites (ca. 2691 Ma), voluminous syn-tectonic tonalites and granodiorites (ca. 2679–2686 Ma) and, rare post–tectonic potassic monzogranite and syenite (ca. 2659–2666 Ma). Metasedimentary rocks include turbidites, epiclastic tuffs, minor iron formation (oxide) and rare volcanic conglomerates. Volcanic rocks of assemblage I include abundant pillowed and massive basalts to andesites with less common silicic lavas, tuffs and volcaniclastic debris flow deposits. Assemblage II contains voluminous silicic tuff and volcaniclastic debris flow deposits but fewer basaltic to andesitic flows. The critical diagnostic feature of the CHSB is the stratigraphic intercalation of compositionally diverse basaltic, andesitic and felsic volcanic rocks throughout both assemblages. Mapping, U–Pb geochronology and lithogeochemistry suggest that an initial MORB-like basaltic plain containing widespread intercalations of dacite to rhyolite was replaced at ca. 2688 Ma by a relatively short-lived, dacite to rhyolite dominated magmatic environment characterized by localized felsic volcanic centres and a bloom of 2686–2679 Ma tonalitic to granodioritic plutons. Basaltic to andesitic rocks are dominated by iron-rich tholeiites, although the proportion of calc-alkaline rocks increases with silica content. Felsic volcanic rocks all exhibit calc-alkaline affinities. The wide range in chemistry of the basaltic to andesitic rocks of both volcanic assemblages implies diverse mantle sources capable of generating voluminous MORB-, with less common ARC-, NEB(OIB)- and rare BABB-like rocks. Similarly, the variable composition of the felsic volcanic rocks indicates both anatexis of eclogitic to garnetiferous mafic crust and also extensive fractionation of mafic precursors in crustal magma chambers. Two geochemically distinct, arc-like mafic suites were generated through contamination of primary mantle-derived magmas

* Corresponding author. Present address: Canada-Nunavut Geoscience Office, 626 Tumitt Building, P.O. Box 2319, Iqaluit, Nunavut X0A 0H0.

E-mail address: hsandema@nrcan.gc.ca (H.A. Sandeman).

0301-9268/$ – see front matter
doi:10.1016/j.precamres.2004.03.014

by juvenile, ca. 2700 Ma silicic crust either in their mantle source or through assimilation upon ascent. ϵNd_t isotopic data are comparable to contemporaneous depleted mantle with only local evidence for incorporation of older, ⋙2700 Ma crust.
The CHSB may have formed via tectono-magmatic processes comparable to those of the Eocene, infant-arcs of the SW Pacific, whereby the formation of a thick sequence of coeval, intercalated, compositionally diverse mantle- and crustal-derived rocks, are generated in an extensional supra-subduction setting. The cessation of supra-subduction zone extension at ca. 2688 Ma, was followed by the short-lived development of felsic volcanic edifices (incipient arc), the extrusion of mafic to felsic magmas and the concomitant intrusion of voluminous syn-kinematic tonalitic plutons. This accompanied a major change in the tectono-magmatic setting accompanying and presumably following the termination of extensional, supra-subduction zone processes.

Keywords: Neoarchaean; Western Churchill Province; Basalts; Rhyolites; Petrogenesis; Geodynamic setting; Infant-arc analogy

1. Introduction

The areally expansive, granite-greenstone terranes of the Western Churchill Province (wCP), lying west and northwest of Hudson Bay (Fig. 1) were originally distinguished from the adjacent Slave and Superior Provinces on the basis of prolific, regional, Paleoproterozoic K–Ar ages (Stockwell, 1982). On the basis of regional aeromagnetic data contrasts, and sparse supporting geological and geochemical data, Hoffman (1988) subdivided the wCP into Rae and Hearne Provinces along the Snowbird Tectonic Zone. Using mapping and lithological reconstructions, but lacking a substantial geochronological and lithogeochemical

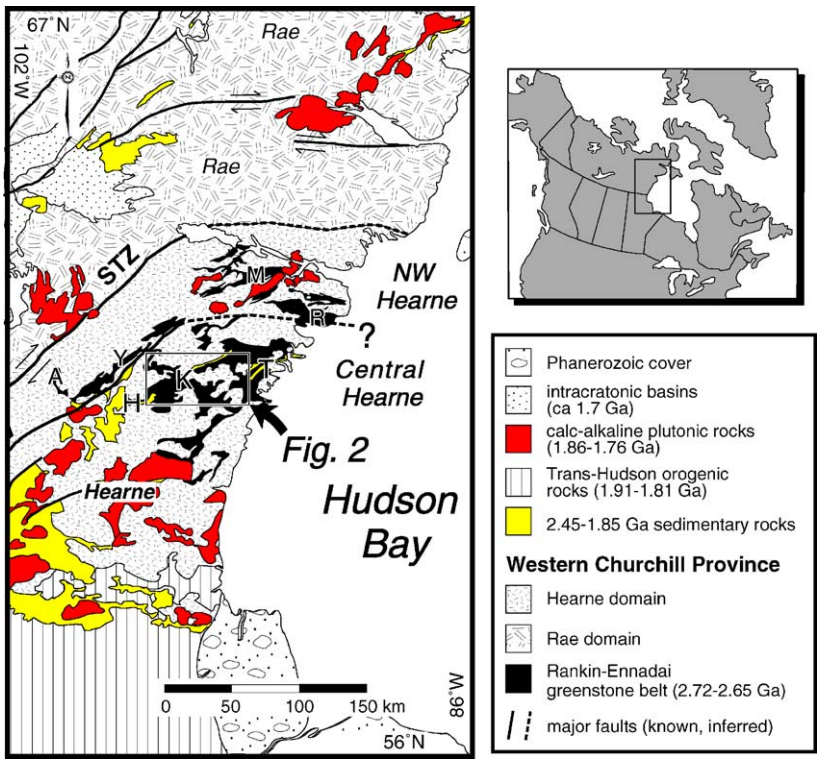

Fig. 1. Simplified geological map of north-central Laurentia showing the location of the study-area relative to the major geological provinces of the NW Canadian Shield. The subdivision of the Hearne domain into NW and central Hearne sub-domains (Hanmer and Relf, 2000) are shown as is the location of Fig. 2. Map modified after Stern and Berman (2000). *Key:* STZ, Snowbird Tectonic zone (Hoffman, 1988); A, Angikuni belt; Y, Yathkyed belt; H, Henik belt; K, Kaminak belt; T, Tavani belt; R, Rankin Inlet belt and; M, MacQuoid belt.

database, Aspler and Chiarenzelli (1996) proposed that the Hearne domain likely formed in an ensimatic setting. Those authors suggested that the Rae represents the marginal, extended continental hinterland and that the Hearne represents either a collapsed marginal basin or a series of laterally accreted volcanic arc–trench systems. Recent, strategically located, field-based, multi disciplinary bedrock mapping projects combined with supporting geoscience studies (Western Churchill NATMAP Project; Hanmer and Relf, 2000) demonstrate that the Hearne Province may be divided into northwestern and central sub-domains (Hanmer and Relf, 2000), distinguished by contrasting Archaean lithological associations and lithogeochemistry but mainly by differences in their latest Neoarchaean and, in particular, Paleoproterozoic tectono-thermal histories (Hanmer and Relf, 2000; Hanmer et al., in press).

The Central Hearne sub-domain contains a series of supracrustal belts, that have been historically referred to from SW to NE as the Henik, Kaminak and Tavani segments (Hanmer et al., in press) but are now collectively referred to as the Central Hearne supracrustal belt (CHSB). This sub-domain covers ca. 30,000 km^2 of the Hearne Province and, as such, represents the second largest Archean greenstone belt after the Abitibi belt of the Superior craton. Despite a substantial history of mineral exploration and a number of proposed, but poorly constrained geodynamic models, only sparse lithogeochemical data for the CHSB is available (cf. Ridler, 1973; Miller and Tella, 1995; Park and Ralser, 1992; Thériault and Tella, 1997; Cousens et al., in press).

This contribution presents lithogeochemical and Nd isotopic data for a wide range of volcanic rocks from the Kaminak segment that, along with lithological and geochronological information, provide petrological tools for the development and testing of plausible geodynamic models for the region (see Cousens et al., in press; Davis et al., 2004; Hanmer et al., in press). Geological field relationships and petrochemical and isotopic data for the Henik segment are addressed by Cousens et al. (in press) whereas the stratigraphy and geochronology of the Tavani segment are discussed in Park and Ralser (1992), Davis and Peterson (1998), Davis et al. (2004) and Hanmer et al. (in press). All ages discussed are ID thermal ionization mass spectrometry determinations on zircon. The database presented herein, comprises complete lithogeochemical analyses for a wide range of volcanic rocks including predominantly basaltic to andesitic pillowed and massive units, as well as common dacitic to rhyolitic rocks.

A fundamental characteristic of the CHSB is the primary (stratigraphic) outcrop to km-scale interlayering, throughout the temporal evolution of the belt, of basaltic to andesitic volcanic rocks and concomitant dacitic to rhyolitic volcanic units of contrasting geochemical affinity. Widespread mafic to intermediate volcanic rocks exhibit five distinct petrochemical subgroups, including MORB-like, arc-like and Nb-enriched basalts throughout, with common, crustally contaminated mafic to intermediate rocks and rare BAB-like basalts. Felsic rocks also comprise five distinct geochemical subgroups, exhibit a continuum from those having characteristics of melts derived from anatexis of eclogite to garnet amphibolite as well as magmas derived from fractionation of mafic precursors. Supporting Nd isotopic data suggest that all the volcanic units are derived from variably depleted, predominantly juvenile Neoarchaean mantle or crust with rare evidence for interaction with significantly older crustal material. In conjunction with companion papers (Cousens et al., in press; Davis et al., 2004; Hanmer et al., in press), we interpret the overall geodynamic setting for the generation of these rocks, in particular those of volcanic assemblage I, to reflect lithospheric processes analogous to those that resulted in extensional, supra-subduction “infant arc” environments of the southwest Pacific ocean during the Eocene (cf. Stern and Bloomer, 1992; Bloomer et al., 1995; Kerrich et al., 1998).

2. Geological setting

2.1. Regional lithological relationships

The CHSB comprises a Neoarchaean, typically well-preserved, greenschist grade mafic metavolcanic dominated supracrustal belt including basalt, andesite, dacite, rhyolite and less common chemical and clastic sedimentary rocks. The volcanic rocks, emplaced between ca. 2681 and 2711 Ma, are cut by voluminous, gabbro to monzogranite plutons that are dominated by tonalite, and collectively range in age from

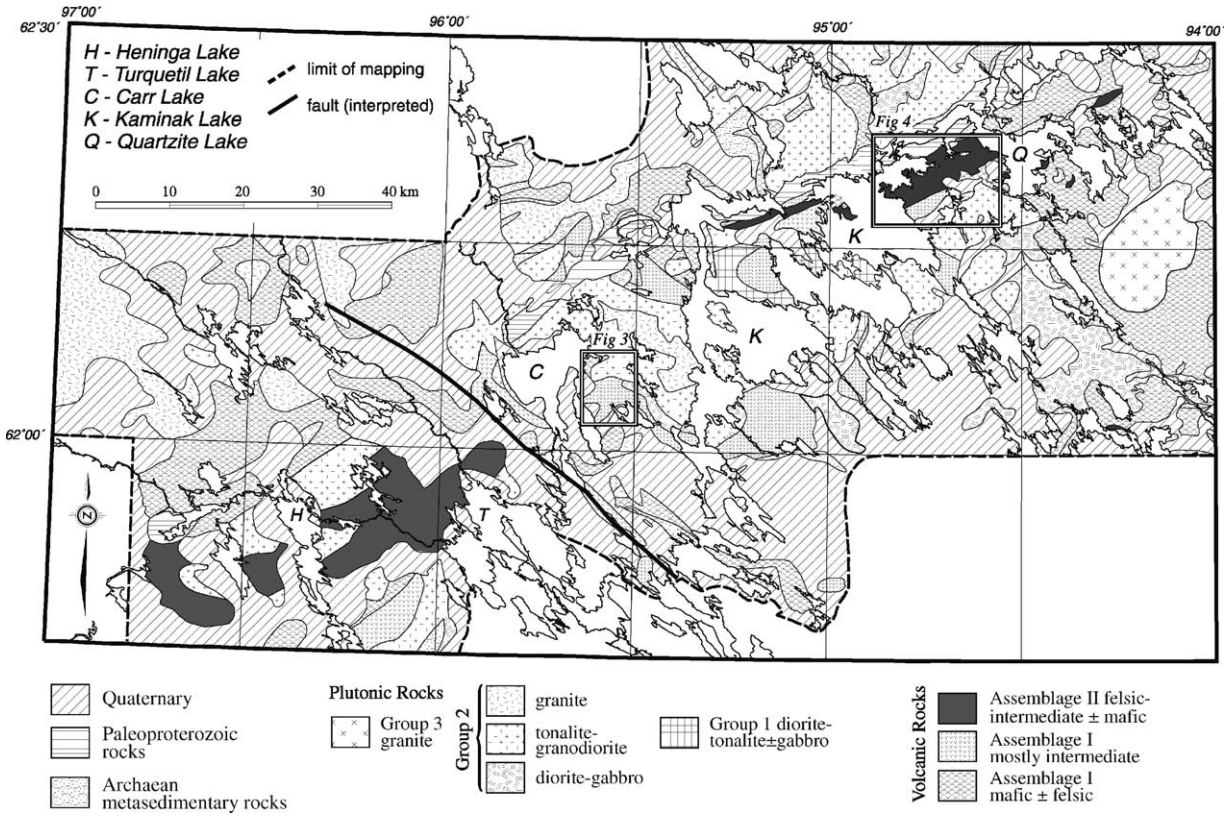

Fig. 2. Simplified geological map of the Kaminak segment of the Central Hearne supracrustal belt from Heninga to Quartzite Lakes. Modified after Hanmer et al., (in press) and Davis et al. (2004). Note the geographical distribution of the volcanic rocks subdivided into assemblages I and II and the location of two detailed map localities.

2659 to 2691 Ma (Davidson, 1970; Mortensen and Thorpe, 1987; Park and Ralser, 1992; Davis et al., 2004; Hanmer et al., in press). The overall outcrop pattern, relative volumes of volcanic rock-types and a discussion of the regional geology and structure of the CHSB are presented elsewhere (Hanmer et al., in press; Cousens et al., in press). One of the fundamental characteristics of the CHSB is the lateral discontinuity of supracrustal map units, a feature that makes it difficult to correlate lithological packages within the belt and to devise a systematic and mappable stratigraphy. Although complex interfingering and on-lapping of volcanic rocks is a feature common to many modern and ancient volcanic terranes (Cas and Wright, 1987; Mueller et al., 1989; Stern et al., 1995), the excellent preservation of igneous textures and the absence of kinematically linked, discrete fault systems suggests that the discontinuity of volcanic rocks in the CHSB is a primary feature reflecting laterally restrictive, short-lived depositional sub-environments (Hanmer et al., in press). Thus, on the basis of lithological correlations and U–Pb geochronology (Hanmer et al., in press; Davis et al., 2004), we subdivide the volcanic rocks of the Kaminak segment into two distinct tectono-magmatic assemblages, the geographical distributions of which are given in Fig. 2.

The older assemblage (assemblage I) spans ca. 20 m.y. (2691–2711 Ma) and comprises a widespread package of pillowed and massive basaltic to andesitic volcanic and volcaniclastic rocks intercalated on the outcrop-scale with subordinate dacitic to rhyolitic lavas, tuffs and less abundant, gabbroic to dioritic sub-volcanic intrusions (Hanmer et al., in press; Sandeman et al., 2004). Collectively, these rocks are inferred to represent an extensive, predominantly mafic sub-aqueous platform. The shorter-lived assemblage II

(2681–2686 Ma), deposited after localized deformation (Davis et al., 2004; Hanmer et al., in press), contains a significantly lower proportion of mafic volcanic rocks that are closely associated with voluminous dacitic to rhyolitic volcaniclastic debris flows, tuffs and lavas and their sub-volcanic and plutonic equivalents. These felsic volcanic dominated sequences of assemblage II are interpreted to represent a series of shallow submarine volcanic edifices (Hanmer et al., in press; Sandeman et al., 2004). Rocks of assemblage I dominate the northwestern and southeastern margins of the map area with rocks of assemblage II occurring as spatially discrete centres constructed on top of the older assemblage and occurring along the north-central axis of the map-area. The partially assembled supracrustal pile was intruded at ca. 2686–2679 Ma by voluminous gabbro–tonalite–monzogranite plutons that dominate the overall geological map pattern (Davidson, 1970; Ridler, 1973; Davis et al., 2004; Hanmer et al., in press). Although overlapping in age with assemblage II volcanic rocks, the majority of these plutons were intruded syn- to late-kinematically with respect to the major, regional deformation event recorded in the area (D2; Hanmer et al., in press). The complete stratigraphy is intruded by widely spaced, potassic, post-tectonic monzogranites (ca. 2666 Ma; Davis et al., 2004) that appear to increase in abundance to the northeast. Moreover, the timing and intensity of the latest Archaean deformation in the CHSB appears to be younger towards the northeast, where it accompanies, or immediately postdates, the intrusion of ca. 2666 Ma granitoids (Park and Ralser, 1992; Davis and Peterson, 1998; Davis et al., 2004).

Although the lithological mapping and geochronological and geochemical database covers a large area, we emphasize that it is the outcrop- to km-scale interrelationships of these rocks that help to underpin the belt-wide tectono-magmatic interpretations. In order to establish the compositional spectrum of the volcanic rocks in the belt, and to delimit distinct packages of supracrustal rocks, geochemical samples were collected from a wide range of rock-types throughout the Kaminak segment of the belt. A number of specific localities, two of which are shown in Figs. 3 and 4, were selected for detailed sampling where primary textures were well preserved. At East Carr Lake and Cache Peninsula (Figs. 3 and 4), basaltic and felsic volcanic rocks with primary features could be widely observed

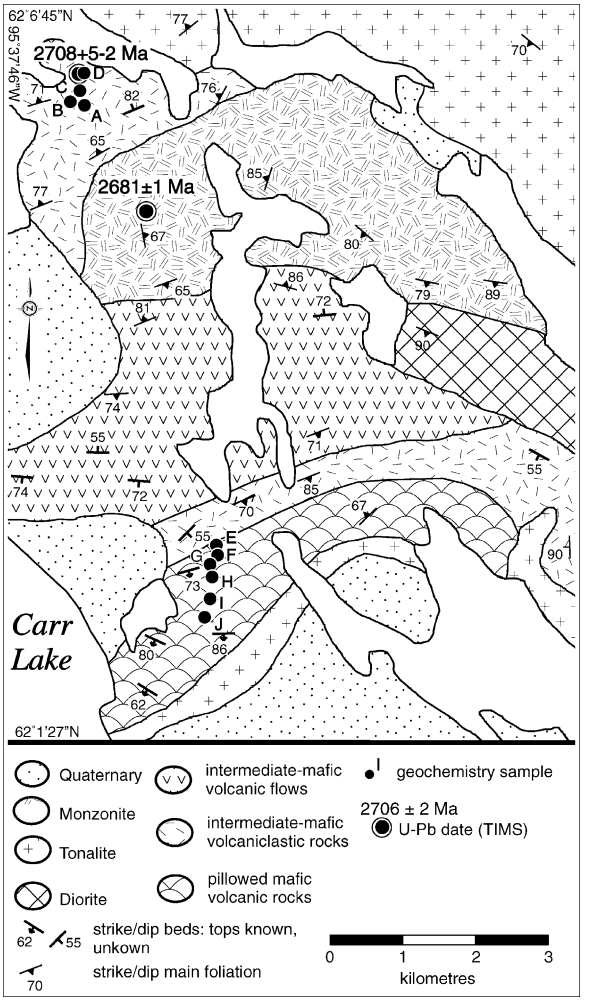

Fig. 3. Geological map of the area at the eastern margin of Carr Lake. Geochemical sample locations are keyed to Fig. 10A. Geochronological data are from Davis et al. (2004).

at the outcrop and km-scale and hence these localities provided a series of geochemical and geochronological targets. Below, we briefly describe the detailed lithological relationships from these two areas.

2.2. Eastern margin of Carr Lake

The volcanic rocks exposed along the eastern margin of Carr Lake (Figs. 2 and 3) comprise a diverse package of mafic through felsic volcanic and volcaniclastic units. In the north, adjacent to a dioritic phase of the ca. 2686 Ma Carr pluton (Davis et al., 2004), a

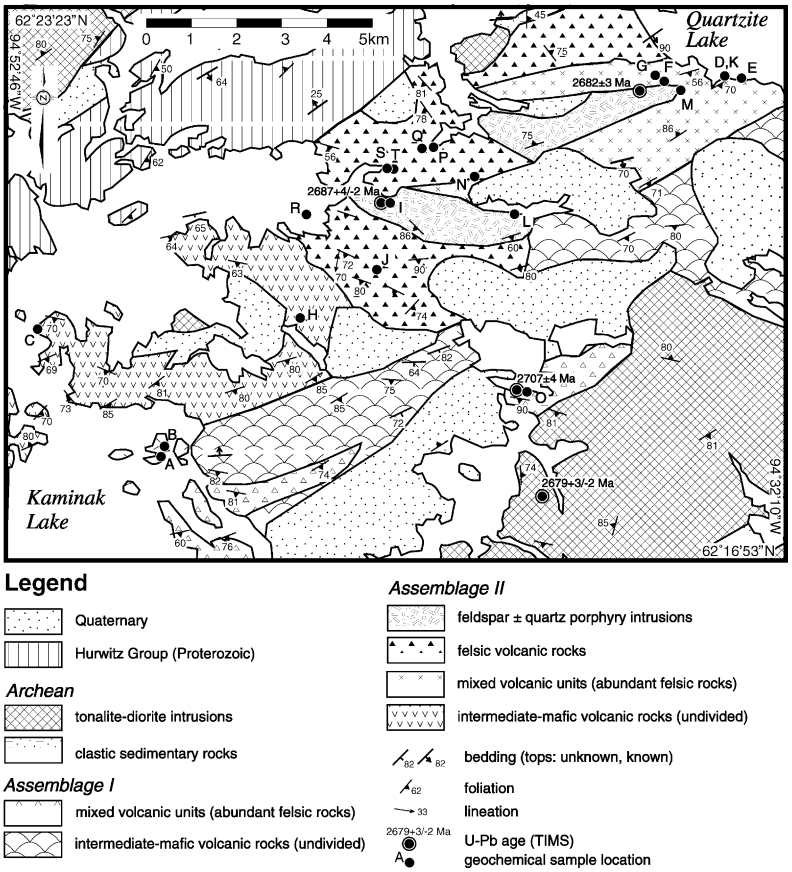

Fig. 4. Geological map of the area lying between NE Kaminak and Quartzite Lakes, herein termed the Cache Peninsula. Geochemical sample locations are keyed to Fig. 10B. Geochronological data are from Davis et al. (2004) and Patterson and Heaman (1990).

series of intermediate to felsic crystal–lapilli tuffs, one of which is dated at 2708^{+5}_{-2} Ma (Davis et al., 2004), are interlayered with generally massive, lower amphibolite facies, amygdaloidal basaltic andesites and intermediate volcaniclastic rocks. To the south, a thick, poorly exposed package of amphibolite facies, fine-grained, massive mafic and intermediate volcanic units pass southward into a thin package of massive, intermediate volcaniclastic rocks and then a thick sequence of pillowed to massive basaltic volcanic rocks. The first two composite units are cross-cut by an arcuate body of hornblende+biotite monzonite dated at 2681 ± 3 Ma (Davis et al., 2004) and considered to represent the youngest intrusive phase of the Carr pluton (Sandeman et al., 2004). The southern package is characterized by small (<40 cm), ovoid to amoeboid, amphibolite-facies grade pillows that yield consistent, southward young-ing directions and no apparent intraformational unconformities. These are intercalated with thick, massive, amphibolite grade basaltic flows and rare, massive felsic horizons that may represent hypabyssal intrusions. This southern sequence is cut by a tonalite correlated with the ca. 2686 Ma Carr pluton (Davis et al., 2004) and hence, the entire East Carr Lake package is interpreted to be part of volcanic assemblage I.

2.3. Cache Peninsula

Cache Peninsula, lying immediately west of Quartzite Lake and bounded to the west by Kaminak Lake, hosts a diverse assemblage of predominantly felsic and intermediate volcanic rocks with abundant, felsic sub-volcanic intrusions (Figs. 2 and 4). Felsic and intermediate tuffs, in particular those exposed in the

south, are commonly extensively sericite and carbonate altered but preserve rare primary features such as angular lithic fragments and lapilli. One such unit, exposed immediately north of the Kaminak pluton (Fig. 4) yielded a U–Pb zircon age of 2707 ± 4 Ma (Davis et al., 2004), indicating that at least some of the rocks belong to volcanic assemblage I. Coring the peninsula are two roughly oval, composite, plagioclase ± quartz ± potassium feldspar pophyritic dacite to rhyolite intrusions. These hypabyssal intrusions yielded two U–Pb ages of 2681 ± 3 Ma (Patterson and Heaman, 1990) and 2687^{+4}_{-2} Ma (Davis et al., 2004), indicating that they belong to volcanic assemblage II. The westernmost porphyry intrusion is flanked to the north and northwest by flow-banded, and commonly autobrecciated quartz-phyric rhyolites and by plagioclase + quartz–phyric massive rhyolite. Dispersed around both porphyry intrusions are a number of coarse-grained, matrix-supported conglomerates containing angular to sub-rounded clasts of predominantly felsic volcanic rocks including flow-banded rhyolite. These "debris flows" probably formed along the flanks of central, subaqueous to possibly subaerial (flow-banded rhyolite), felsic volcanic centres (cf. Rainbird and Hadlari, 1998).

The pophyritic intrusions intrude a distinct package of broadly contemporaneous interlayered felsic, intermediate and mafic volcanic rocks. The mafic flows in this package are locally silicified and sericitised but commonly comprise well-preserved, amygdaloidal and vesicular, pillowed and massive basalts to andesites. Pillows in these flows are typically 50–80 cm in diameter, have cm-scale black–brown selvedges and indicate southwestward younging.

3. Geochemistry

Below, we discuss the overall geochemical characteristics of the volcanic rocks of the Kaminak segment of the CHSB including their major and trace element variations and Nd isotopic compositions. We emphasize that the study is regional and reconnaissance in nature and some volcanic sequences (e.g., Victory Lake; Davis et al., 2004; Hanmer et al., in press) are not proportionally represented in our dataset. In order to underscore their chemical heterogeneity, in the following sections we subdivide the volcanic rocks into their respective assemblages, and into five distinct mafic and felsic subgroups on the basis of their multielement profiles (see Section 3.3 below).

3.1. Sampling and alteration

One hundred and fifty three whole-rock specimens of mafic to felsic volcanic and hypabyssal intrusive rocks were collected from throughout the map area, with subgroups obtained from a number of well exposed volcanic packages (e.g., Figs. 2–4; Tables 1–3). Wherever possible, the cores of pillows were sampled in the mafic rocks, although locally abundant, massive mafic rocks made this approach difficult. Intermediate rocks were also problematic for sampling as they typically occur as coarse lithic tuffs or volcaniclastic debris flows. Felsic units are also under-represented as they commonly exhibit extensive sericite-quartz–ankerite alteration. Hence, the number of analyses of andesitic to rhyolitic rocks presented herein are not representative of their actual volume. Analytical methods for the whole-rock geochemical and Nd isotopic analyses are presented in Appendix A.

Extensive hydrothermal alteration of subaqueous volcanic rocks is a common phenomenon, typically characterized by selective chemical modifications including high LOI values, scatter and inconsistency of major element data, and addition or subtraction of the large ion lithophile (LILE) elements such as Li, Rb, Sr, and Ba. High field strength (HFSE) and rare earth (REE) elements in such rocks are, however, essentially immobile under most fluid–rock interactions (e.g., Pearce and Cann, 1973; Wood et al., 1979; Middelburg et al., 1988). Herein, we outline the major and trace element geochemistry of the volcanic rocks of the Kaminak segment but emphasize, in particular, their HFSE and REE variations.

3.2. Major and trace element variations

Volcanic rocks of the study-area, incorporating those from both assemblages, range from rare picritic basalts through to rhyolites (Fig. 5A; LeBas et al., 1986) an observation corroborated by the immobile trace element discrimination plot of Winchester and Floyd (1977; modified after Pearce, 1996; Fig 5B). A total of five specimens are picro-basalts, 70 are basalts, 21 are basaltic andesites, 17 andesites, 24 dacites and

Table 1
Salient lithogeochemical characteristics of basaltic to andesitic and dacitic to rhyolitic rock-types of the Kaminak segment

	Assemblage	#Analyses	Mg#	Nb (ppm)	TiO_2 (wt.%)	Th_N/La_N	Th_N/Nb_N	La_N/Nb_N	La_N/Yb_N	La_N/Sm_N	Gd_N/Yb_N	Eu/Eu* (ppm)	∑REE	ϵNd_t
Mafic														
MAF-1	I and II	67	28–63	2.4–7.7	0.3–0.6	0.57–0.98	0.6–1.0	0.8–1.5	0.7–1.7	0.7–1.2	1.0–1.6	0.58–1.11	29–80	2.0–3.5
MAF-2	II and I	19	30–67	1.6–10.0	0.5–1.8	0.95–2.20	2.0–6.4	1.5–3.2	2.2–12.1	1.5–3.8	1.0–1.9	0.64–1.02	33–163	0.6–2.3
MAF-3	I and II	11	18–62	5.4–17.0	0.65–1.4	0.52–0.85	1.4–2.5	1.8–4.7	3.7–11.2	1.9–3.5	1.4–2.1	0.77–0.96	93–192	0.6–2.1
MAF-4	I	3	56–63	1.3–3.4	0.6–0.9	0.87–0.88	1.1–1.2	1.3–1.4	0.8–2.1	0.8–1.4	1.1–1.5	0.96–1.01	21–38	2.9
MAF-5	I and II	10	34–58	8.8–15.0	1.1–1.8	0.49–0.74	0.6–1.1	1.2–1.8	1.4–7.7	1.0–2.6	1.3–2.3	0.76–0.97	82–139	1.1–3.4
Felsic														
FEL-1	I and II	10	31–55	1.9–7.3	0.16–0.35	0.86–1.4	2.7–8.8	2.3–7.3	13.5–54.2	2.5–6.8	2.6–4.3	0.69–1.01	33–93	1.6
FEL-2	II	3	31–57	1.7–12	0.38–0.59	0.75–0.84	1.6–7.4	2.1–8.8	18.8–26.0	3.8–4.2	2.7–3.8	0.95–1.02	71–118	na
FEL-3	I and II	8	36–58	6.5–11.6	0.36–0.94	1.2–2.0	2.4–3.2	1.5–2.4	4.7–10.4	2.6–3.7	1.1–2.1	0.84–1.04	48–138	2.9
FEL-4	I and II	11	10–63	7.2–24.0	0.06–0.43	0.9–3.9	2.4–10.6	1.3–4.6	2.8–8.7	1.9–4.1	0.9–1.6	0.23–0.66	103–331	0.2–2.6
FEL-5	II	2	51–60	18.0–19.0	<0.10	3.8–4.2	2.3–2.4	0.5–0.6	1.2–1.3	1.1	1.0–1.2	0.38–0.50	95–109	1.7

Note: subscript N indicates values are chondrite normalized (Sun and McDonough, 1989), subscript *t* indicates ϵNd value calculated (DePaolo, 1981) at time $t = 2690$ Ma. Ranges given are absolute ranges for each petrological group.

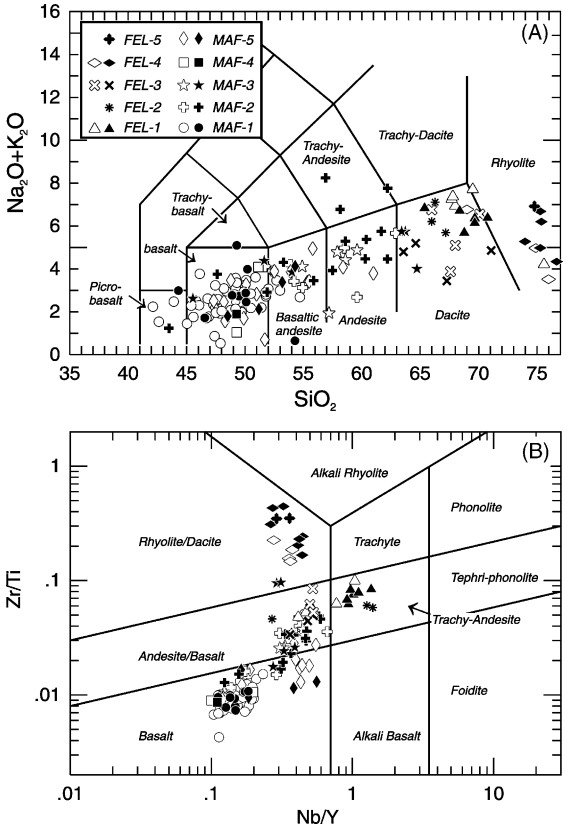

Fig. 5. (A) Total alkalies vs. SiO_2 (LeBas et al., 1986) for volcanic and volcaniclastic rocks of the Kaminak segment of the CHSB. (B) Zr/Ti vs. Nb/Y diagram of Winchester and Floyd (1977) modified according to Pearce (1996). Open symbols are specimens from volcanic assemblage I, whereas solid symbols are from assemblage II. Where ages are unknown, samples are correlated on the basis of texture and lithostratigraphic association. Rocks have also been further subdivided into five mafic and felsic subgroups on the basis of their multielement profiles (see below).

16 rhyolites. Basaltic rocks are significantly more abundant in volcanic assemblage I, whereas dacitic and rhyolitic rocks are more prominent in assemblage II. For simplicity, further discussion of the volcanic rocks is undertaken with reference to their bulk composition; hence, we outline separately, the characteristics of the basaltic to andesitic rocks and the dacitic to rhyolitic rocks.

The basaltic to andesitic rocks of both assemblages are divided into tholeiites characterized by an iron enrichment trend and increasing TiO_2 with fractionation, and transitional calc-alkaline to calc-alkaline

Table 2
Whole-rock geochemical data for 20 representative basaltic to andesitic volcanic rocks of the Kaminak segment

Sample	HS420	HS426	HS423	HS540	HS424	HS451	HS421	HS541	HS431A	HS517
Group[a]	1	1	1	1	1	1	2	4	1	1
Rock-Type[b]	P (I)	P (I)	P (I)	M (I)	P (I)	M (I)	P (II)	P (I)	P (I)	P (I)
Easting[c]	420354	426288	420053	422350	420005	405628	420382	422601	440097	381047
Northing[c]	6920430	6921856	6919739	6933300	6919678	6909244	6919897	6933237	6889487	6862084
Zone[c]	15	15	15	15	15	15	15	15	15	15
SiO_2	42.12	42.63	45.04	46.07	46.13	47.33	47.64	49.30	49.60	50.05
TiO_2	1.17	1.06	1.26	1.25	1.23	1.10	0.90	0.56	1.11	1.34
Al_2O_3	14.05	12.52	9.89	12.12	14.06	12.10	14.62	14.90	15.80	12.51
$Fe_2O_3^T$	17.45	15.75	18.99	15.95	14.53	18.72	13.49	10.40	14.10	15.99
MnO	0.28	0.24	0.25	0.20	0.22	0.23	0.18	0.14	0.22	0.36
MgO	9.70	11.85	9.28	11.50	8.14	6.97	7.05	9.02	5.17	4.18
CaO	8.36	10.19	9.15	7.57	6.75	7.14	8.23	10.76	10.72	12.91
Na_2O	1.90	1.39	1.34	2.26	3.59	2.33	2.68	1.00	1.90	2.21
K_2O	0.34	0.15	0.11	0.05	0.18	0.18	1.07	0.04	0.18	0.28
P_2O_5	0.07	0.08	0.16	0.10	0.08	0.09	0.13	0.04	0.08	0.08
LOI	2.85	2.75	3.74	3.00	2.90	2.41	1.99	3.00	0.90	1.59
Total	98.29	98.61	99.21	100.07	97.81	98.60	97.98	99.16	99.78	101.50
Mg#	52	60	49	59	53	43	51	63	42	34
Cr	398	390	223	278	417	19	115	430	330	35
Ni	146	131	78	86	139	18	114	140	130	32
Co	na	na	na	na	na	na	na	49	65	na
Sc	41	47	48	49	47	50	30	40	49	61
V	343	342	357	382	350	418	200	220	340	393
Cu	14	36	61	89	135	95	85	90	92	101
Pb	1.4	0.8	1.2	1.1	0.6	0.6	7.5	1.5	2.0	4.0
Zn	79	63	98	73	71	80	67	63	87	83
Rb	4.3	1.3	1.6	0.3	1.7	3.0	17.0	0.2	1.8	4.6
Cs	0.20	0.04	0.24	0.03	0.04	0.16	0.51	0.03	0.18	0.07
Ba[d]	129	32	30	12*	82	22	857	16	37*	178
Sr	122	124	100	103	94	128	242	130	140	99
Ga	20	18	15	17	18	19	18	14	18	20
Ta	0.20	0.21	0.46	0.27	0.21	0.41	0.42	0.08	0.19	0.26
Nb	3.3	3.0	6.3	3.8	3.1	6.1	5.8	1.3	2.9	3.9
Hf	1.1	1.6	1.7	1.7	1.3	2.2	3.2	0.6	1.4	1.1
Zr	74	71	115	79	74	110	104	30	66	83
Y	21	20	27	27	23	32	18	13	26	26
Th	0.22	0.28	0.69	0.38	0.27	0.68	3.70	0.17	0.30	0.38
U	0.06	0.06	0.16	0.08	0.08	0.16	0.86	0.09	0.10	0.06
La	3.17	3.13	7.15	4.33	3.35	6.97	15.62	1.60	3.50	4.36
Ce	8.92	8.64	18.60	11.34	9.41	17.61	32.13	4.60	9.50	11.74
Pr	1.44	1.42	2.75	1.78	1.54	2.65	4.01	0.68	1.50	1.88
Nd	7.32	7.22	13.68	9.20	7.95	12.72	16.38	3.80	7.80	9.44
Sm	2.54	2.47	4.01	2.86	2.72	3.89	3.64	1.30	2.60	3.07
Eu	1.03	0.89	1.30	1.02	0.99	1.20	1.21	0.52	0.90	1.05
Gd	3.46	3.68	5.09	4.08	3.72	5.18	3.63	1.90	3.70	4.17
Tb	0.58	0.59	0.86	0.69	0.65	0.88	0.59	0.35	0.69	0.70
Dy	4.07	4.08	5.61	4.64	4.40	5.83	3.73	2.20	4.30	4.93
Ho	0.88	0.87	1.17	1.02	0.93	1.23	0.72	0.49	0.93	1.06
Er	2.54	2.53	3.46	3.14	2.72	3.70	2.15	1.50	2.70	3.04
Tm	0.37	0.37	0.46	0.45	0.42	0.54	0.32	0.22	0.40	0.45
Yb	2.30	2.34	3.04	2.99	2.51	3.37	2.00	1.50	2.90	3.07
Lu	0.30	0.34	0.41	0.43	0.35	0.48	0.31	0.22	0.41	0.47

Table 2 (*Continued*)

Sample	HS530	HS432	HS444A	RR174B	HS58C	HS445	HS58B	HS433	HS435	HS125A
Group[a]	1	1	5	3	3	5	3	5	2	2
Rock-type[b]	P (II)	P (I)	P (I)	P (II)	M (I)	P (I)	M (I)	P (I)	P (I)	M (II)
Easting[c]	654858	440358	365059	418253	363690	365215	363670	439537	439017	345742
Northing[c]	6870928	6889404	6882865	6916353	6888930	6882465	6888954	6880819	6880391	6870761
Zone[c]	14	15	15	15	15	15	15	15	15	15
SiO_2	50.06	51.40	53.90	54.02	54.90	55.50	57.20	58.40	59.60	60.40
TiO_2	1.04	1.12	1.41	1.42	0.78	1.44	0.78	1.08	0.88	0.67
Al_2O_3	12.57	15.80	17.50	13.35	15.60	16.20	14.70	14.60	15.60	16.80
$Fe_2O_3{}^T$	13.59	12.20	8.10	9.68	9.10	9.70	8.60	9.00	7.40	7.10
MnO	0.30	0.20	0.12	0.15	0.18	0.19	0.14	0.14	0.11	0.11
MgO	5.83	5.18	4.92	5.19	7.37	3.94	6.10	4.54	3.47	3.86
CaO	9.27	11.15	9.12	6.48	6.71	9.37	10.36	7.37	9.81	4.63
Na_2O	2.55	2.00	3.40	3.76	3.70	3.10	1.50	3.80	2.50	3.80
K_2O	0.33	0.20	0.48	0.09	0.41	0.32	0.44	0.28	0.18	1.58
P_2O_5	0.05	0.09	0.25	0.24	0.29	0.29	0.29	0.30	0.20	0.14
LOI	3.10	0.70	0.60	3.92	1.30	0.30	0.40	0.30	0.50	1.80
Total	98.69	100.04	99.80	98.30	100.34	100.35	100.51	99.81	100.25	100.89
Mg#	46	46	55	52	62	45	58	50	48	52
Cr	181	310	170	16	202	460	197	270	130	66
Ni	72	130	99	25	107	260	118	140	78	57
Co	na	56	44	na	30	55	32	48	35	23
Sc	44	46	25	30	25	25	25	24	18	16.0
V	319	320	190	187	150	170	171	160	130	106
Cu	106	110	29	33	18	15	88	36	23	18
Pb	0.4	2.0	2.0	2.3	2.0	2.0	3.0	2.0	2.0	2.0
Zn	61	73	35	87	89	71	82	84	84	68
Rb	5.1	2.7	15.0	1.7	17.0	4.4	6.5	6.2	5.8	30.0
Cs	0.03	0.28	0.60	0.13	1.20	0.11	0.28	0.22	0.07	0.38
Ba[d]	142	65*	130*	56	67	130*	180	140*	na	na
Sr	104	85	240	186	130	300	94	160	320	197
Ga[e]	16	18	18	21	14	16	17	17	20	18
Ta	0.17	0.19	0.60	0.79	0.36	0.46	0.38	0.53	0.45	0.40
Nb	2.9	3.3	11.0	12.9	5.5	11.0	5.9	9.9	8.9	5.7
Hf	1.1	1.7	3.3	4.7	2.7	2.8	2.7	3.0	3.4	4.6
Zr	58	66	145	222	120	157	120	130	181	141
Y	20	28	26	33	18	25	18	23	20	12
Th	0.25	0.36	1.10	2.15	1.60	1.10	1.50	1.30	2.10	1.80
U	0.05	0.13	0.31	0.48	0.37	0.29	0.34	0.35	0.54	0.45
La	2.72	3.60	13.00	22.01	25.02	16.00	21.00	17.00	18.00	13.00
Ce	7.81	10.00	33.00	48.93	61.00	39.00	51.02	43.00	40.00	26.00
Pr	1.27	1.60	4.50	6.58	7.91	5.40	6.60	5.50	4.80	3.10
Nd	6.69	8.30	21.00	26.20	30.02	24.00	26.00	24.00	19.00	12.00
Sm	2.22	2.90	4.60	5.97	5.01	5.20	4.60	5.10	4.20	2.40
Eu	0.75	0.97	1.40	1.79	1.41	1.60	1.20	1.50	1.30	0.76
Gd	3.12	3.90	4.60	6.46	4.01	5.10	3.60	4.80	4.10	2.30
Tb	0.54	0.70	0.72	1.02	0.54	0.78	0.52	0.77	0.66	0.35
Dy	3.68	4.70	4.40	6.23	3.11	4.40	3.00	4.20	3.40	2.00
Ho	0.81	1.00	0.87	1.22	0.58	0.86	0.61	0.83	0.68	0.40
Er	2.35	2.80	2.40	3.47	1.60	2.50	1.70	2.40	2.00	1.00
Tm	0.34	0.46	0.36	0.50	0.25	0.34	0.25	0.33	0.29	0.16
Yb	2.08	3.00	2.30	2.97	1.61	2.40	1.71	2.30	2.00	1.10
Lu	0.29	0.46	0.38	0.49	0.27	0.34	0.28	0.33	0.28	0.17

Key: Major elements in wt.% oxide, trace elements in ppm. All iron is given as total Fe_2O_3 ($Fe_2O_3{}^T$). LOI, loss on ignition; na, not analysed; bd, below detection.

[a] Geochemical group according to their extended incompatible element profile (see text).

[b] P, pillowed flow; M, massive flow; D, synvolcanic dyke; (I) assemblage I; (II) assemblage II.

[c] UTM coordinates in NAD 27 projection.

[d] All analyses by XRF except marked by * are by ICPOES.

[e] All analyses by XRF except marked by * are by ICPMS.

Table 3
Whole-rock geochemical data for nine representative felsic volcanic rocks of the Kaminak segment

Sample	SH375	HS151	JR062a	HS496A	TP10A	HS92	HS057	HS416A	HS527A
Group[a]	2	3	3	1	1	4	4	4	5
Rock-type[b]	DAC (II)	DAC (I)	ASHTUFF (I)	QFP (II)	RHY (II)	RHY (I)	RHYtuff (I)	RHY (I)	RHYbrecc (II)
Easting[c]	409003	413288	425371	412895	410086	349520	363447	392602	411355
Northing[c]	6913940	6910029	6909506	6913840	6912818	6884758	6889448	6908789	6914893
SiO_2	66.30	67.60	68.00	68.80	70.80	74.90	76.00	77.60	77.90
TiO_2	0.59	0.36	0.62	0.31	0.26	0.21	0.32	0.07	0.06
Al_2O_3	17.70	11.74	15.10	14.50	14.80	11.60	10.80	12.10	12.50
$Fe_2O_3{}^T$	4.10	6.41	4.80	2.70	2.20	2.50	2.10	1.10	0.60
MnO	0.02	0.10	0.09	0.02	0.04	0.04	0.04	0.02	0.00
MgO	0.92	3.65	1.36	0.72	0.73	2.13	0.48	0.20	0.32
CaO	1.41	2.96	3.23	3.08	2.53	1.09	4.80	0.61	0.27
Na_2O	5.40	3.50	3.30	2.40	4.50	0.80	0.70	4.20	2.10
K_2O	1.71	0.38	1.80	3.29	1.88	4.17	2.82	2.56	5.28
P_2O_5	0.23	0.08	0.13	0.10	0.08	0.03	0.06	0.02	0.00
LOI	1.70	2.82	1.70	4.00	4.00	2.00	1.00	1.00	0.90
Total	100.08	99.60	100.13	99.92	101.82	99.47	99.12	99.48	99.93
Cr	26	40	34	15	bd	13	bd	16	bd
Ni	bd	20	15	bd	bd	bd	bd	bd	bd
Co	15	na	8	12	5	bd	bd	bd	31
Sc	5.0	9.0	9.5	4.3	2.5	5.9	7.4	2.9	2.3
V	31	48	58	23	12	10	9	bd	bd
Cu	16	26	23	bd	bd	17	17	bd	bd
Pb[d]	2.0	1.5	4	bd	3.0	5.0	4.0	2.0	2.0
Zn	78	36	76	26	46	41	26	10	29
Rb	40	13	65	63	51	78	67	78	96
Cs	1.60	0.50	1.10	2.10	4.20	1.60	0.42	1.10	2.00
Ba	350	150	260	580	310	3400	420	520	510
Sr	240	122	230	95	220	42	120	43	23
Ga[d]	23	14	19*	19*	19*	12	12	14	18
Ta	0.60	1.01	0.74	0.40	0.40	1.30	0.89	0.80	1.70
Nb	12.0	7.6	11.00	6.7	5.3	12.0	12.0	12.0	19.0
Hf	4.7	4.5	5.80	na	3.1	6.6	7.2	3.3	5.1
Zr	205	183	230	154	130	234	282	102	126
Y	9	14	22.00	6.9	4	32	33	27	53
Th	2.20	2.85	3.70	2.20	1.90	6.60	4.50	10.00	5.10
U	0.73	0.73	0.85	0.69	0.58	1.50	1.00	2.20	0.90
La	24.00	17.23	24.0	19.0	18.00	33.00	26.00	21.00	9.90
Ce	52.00	34.99	51.0	38.0	35.00	69.00	57.00	42.00	25.00
Pr	6.20	3.94	5.90	4.0	3.90	7.60	6.90	4.60	3.70
Nd	24.00	15.04	22.0	15.0	14.00	29.00	26.00	17.00	18.00
Sm	4.00	3.02	4.30	2.6	1.90	6.20	5.40	3.30	6.00
Eu	1.10	0.84	1.20	0.65	0.46	0.46	1.10	0.34	1.10
Gd	3.10	2.98	4.00	2.00	1.30	6.10	5.10	3.30	7.70
Tb	0.40	0.45	0.62	0.26	0.14	0.98	0.84	0.62	1.40
Dy	1.80	2.70	3.50	1.30	0.71	5.30	4.80	3.60	8.70
Ho	0.31	0.57	0.71	0.22	0.13	1.10	1.10	0.85	1.80
Er	0.67	1.72	1.90	0.54	0.29	2.90	3.00	2.60	5.00
Tm	0.09	0.26	0.29	0.08	0.04	0.48	0.51	0.41	0.76
Yb	0.67	1.66	2.00	0.52	0.26	3.30	3.50	3.10	5.40
Lu	0.09	0.25	0.31	0.08	0.04	0.56	0.57	0.47	0.74

Note: Major elements in wt.% oxide, trace elements in ppm. All iron is given as total Fe_2O_3 ($Fe_2O_3{}^T$). LOI, loss on ignition; na, not analysed; bd, below detection.

[a] Geochemical group according to their extended incompatible element profile (see text).

[b] DAC, dacite; ASHTUFF, ashflow tuff; QFP, quartz-feldspar porphyry; RHY, rhyolite flow; RHYtuff, rhyolite tuff; RHYbrecc, rhyolite breccia; (I), assemblage I; (II), assemblage II.

[c] UTM coordinates in zone 15, NAD 27 projection.

[d] All analyses by ICPMS, except those marked by * are by XRF.

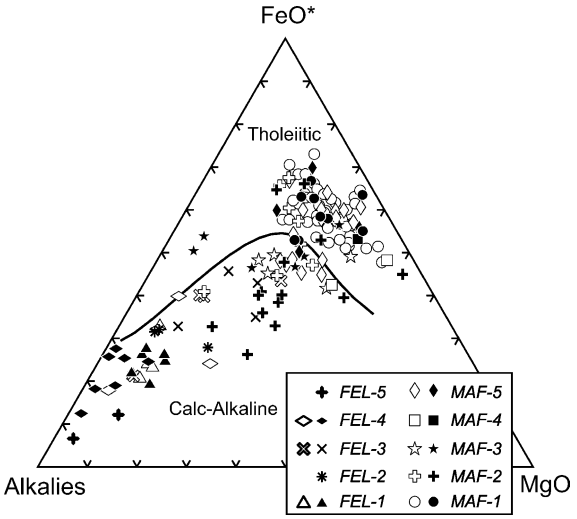

Fig. 6. AFM diagram (Irvine and Barager, 1971) volcanic and volcaniclastic rocks of the Kaminak segment. Symbols as in Fig. 5.

rocks having no iron enrichment trend and essentially constant TiO_2 (Irvine and Barager, 1971; Miyashiro, 1974) with fractionation (Fig. 6). Tholeiitic rocks predominate, particularly in assemblage I, and typically have lower silica contents than the calc-alkaline rocks. Within each volcanic assemblage, samples do not exhibit systematic inter-element relationships, suggesting the presence of multiple mafic magma suites.

Magnesium numbers (Mg#'s: molecular (MgO/FeO^T + MgO) × 100) and Cr and Ni contents of most of the tholeiitic rocks are generally too low for these to represent magmas that could have equilibrated with peridotitic mantle (Roeder and Emslie, 1970) (Tables 1 and 2). A few tholeiitic specimens from both assemblages, however, have elevated Mg#'s (#67), Cr (#1059 ppm) and Ni (#396 ppm), indicating that some rocks have been directly derived from peridotitic mantle. Overall, the majority of the tholeiitic rocks appear, however, to have undergone subsequent fractionation in crustal magma chambers. The Mg#'s (50–66), Cr (16–325 ppm) and Ni (25–155 ppm) contents of the calc-alkaline rocks fall within the range for those of the tholeiitic rocks, however, the former commonly exhibit higher Mg#'s at comparable SiO_2 contents, presumably reflecting their lack of iron enrichment with fractionation.

With the exception of Cr and Ni, major and trace elements for tholeiitic basaltic to andesitic rocks of both assemblages exhibit negative, roughly linear or scattered relationships to Mg# (e.g., Fig. 7A–D). Basaltic to andesitic calc-alkaline rocks of both assemblages, however, exhibit generally scattered covariation for most elements versus Mg#. In particular, the HFSE and immobile trace elements exhibit either weak negative or scattered covariation with Mg#. P_2O_5, TiO_2, Nb, Y, Zr, Hf and Ta concentrations for the calc-alkaline rocks are highly variable (e.g., ± 0.2 wt.% P_2O_5 at equivalent Mg#'s). Tholeiitic samples exhibit positive linear trends on log Nb, Y and TiO_2 versus log Zr plots (cf. Pearce and Norry, 1979), whereas the calc-alkaline rocks exhibit more scattered trends with apparent decreases in Y and TiO_2. Although all of the tholeiites are clearly not cogenetic, these empirical observations suggest that they were generated by the removal of olivine + clinopyroxene ± plagioclase from more primitive melts. Variations of these elements for the calc-alkaline rocks, however, indicate that other mineral phases, possibly hornblende, magnetite or biotite were fractionated from their primitive melts. Moreover, a pronounced variability in the abundances of the HFSE suggests that the calc-alkaline rocks of either assemblage are not petrogenetically linked through simple processes and hence the variability is probably also a function of mantle source heterogeneity and/or varying amounts of crustal contamination during ascent.

Intermediate and felsic volcanic rocks from both assemblages range from dacites through rhyolites (Fig. 5A and B) although a number of these are trachy-andesites and exhibit higher than average Nb/Y (Pearce, 1996). Dacitic and rhyolitic rocks all exhibit calc-alkaline characteristics (Fig. 6). These felsic rocks appear to form two distinct clusters, irrespective of their stratigraphic setting, on most bivariate plots that use SiO_2 as a fractionation index. The first is characterized by SiO_2 ranging from 63.5 to 71.1 wt.% and the second by SiO_2 varying from 74.0 to 78.6 wt.% (Fig. 7E and F). The former are characterized by highly variable abundances of most elements whereas the latter are typified by a tight coherence for most of the major elements, but significant variation in the trace and, in particular the strongly incompatible elements. These features imply that no simple petrogenetic processes can easily explain the elemental variations exhibited by the dacitic to rhyolitic rocks of both volcanic assemblages of the Kaminak segment.

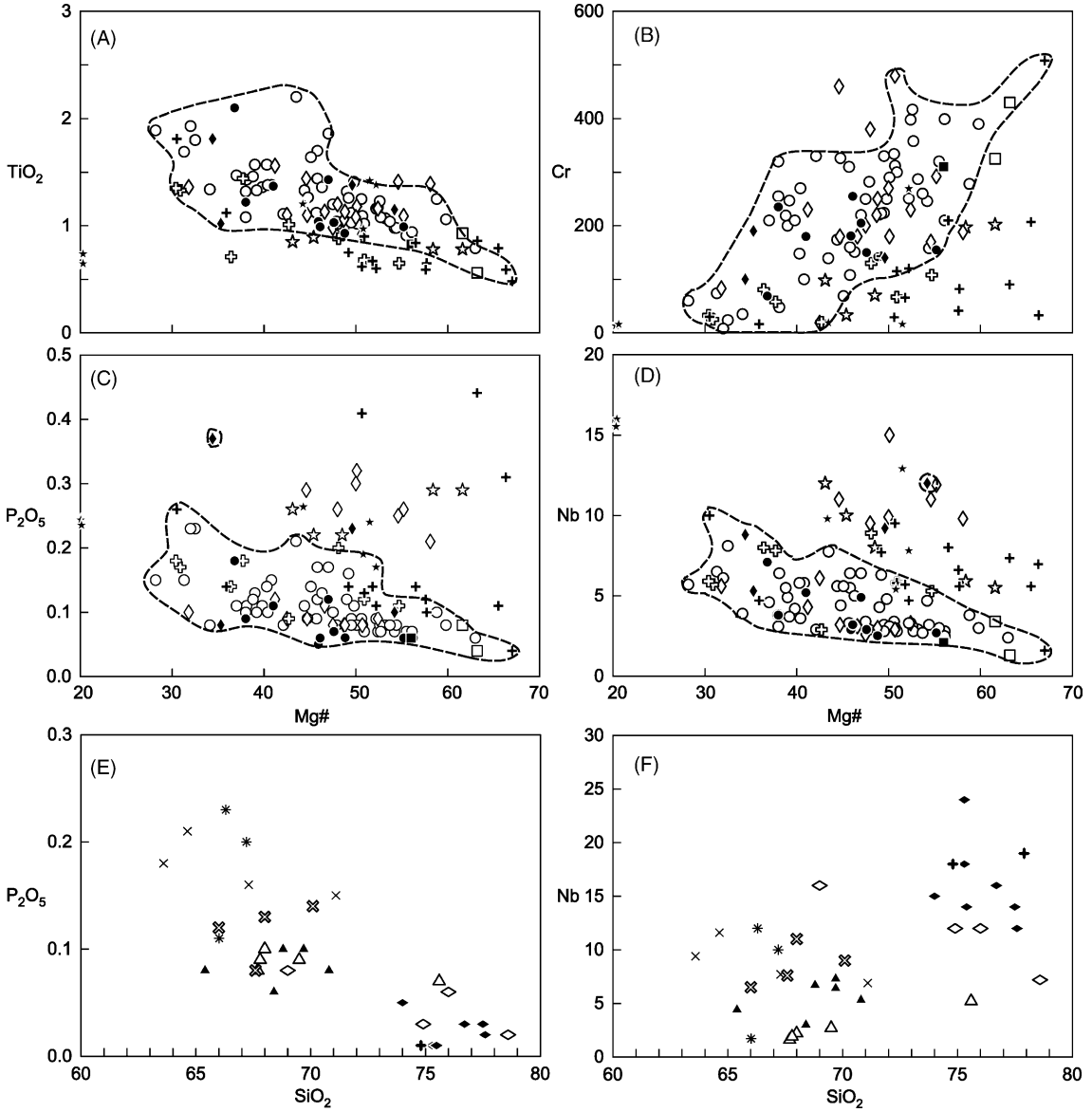

Fig. 7. A through D are plots of selected major and trace element data vs. Mg# for basaltic to andesitic rocks of the Kaminak segment. Tholeiitic samples are outlined by the dashed fields. Figures E and F are plots of high field strength elements (HFSE) vs. SiO_2 for intermediate to felsic rocks. Symbols as in Fig. 5.

3.3. Multielement plots

Primitive mantle (PM) normalized (Sun and McDonough, 1989), multielement plots for all volcanic rocks of the Kaminak segment are shown in Figs. 8 and 9 and salient petrochemical features are presented in Tables 1–3. Negative P anomalies of variable magnitude are typical of the mafic-intermediate rocks of the region, a feature that we interpret here as a result of an overestimation of the primitive mantle normalization value by Sun and McDonough (1989). Tholeiitic, basaltic to andesitic rocks are generally characterized

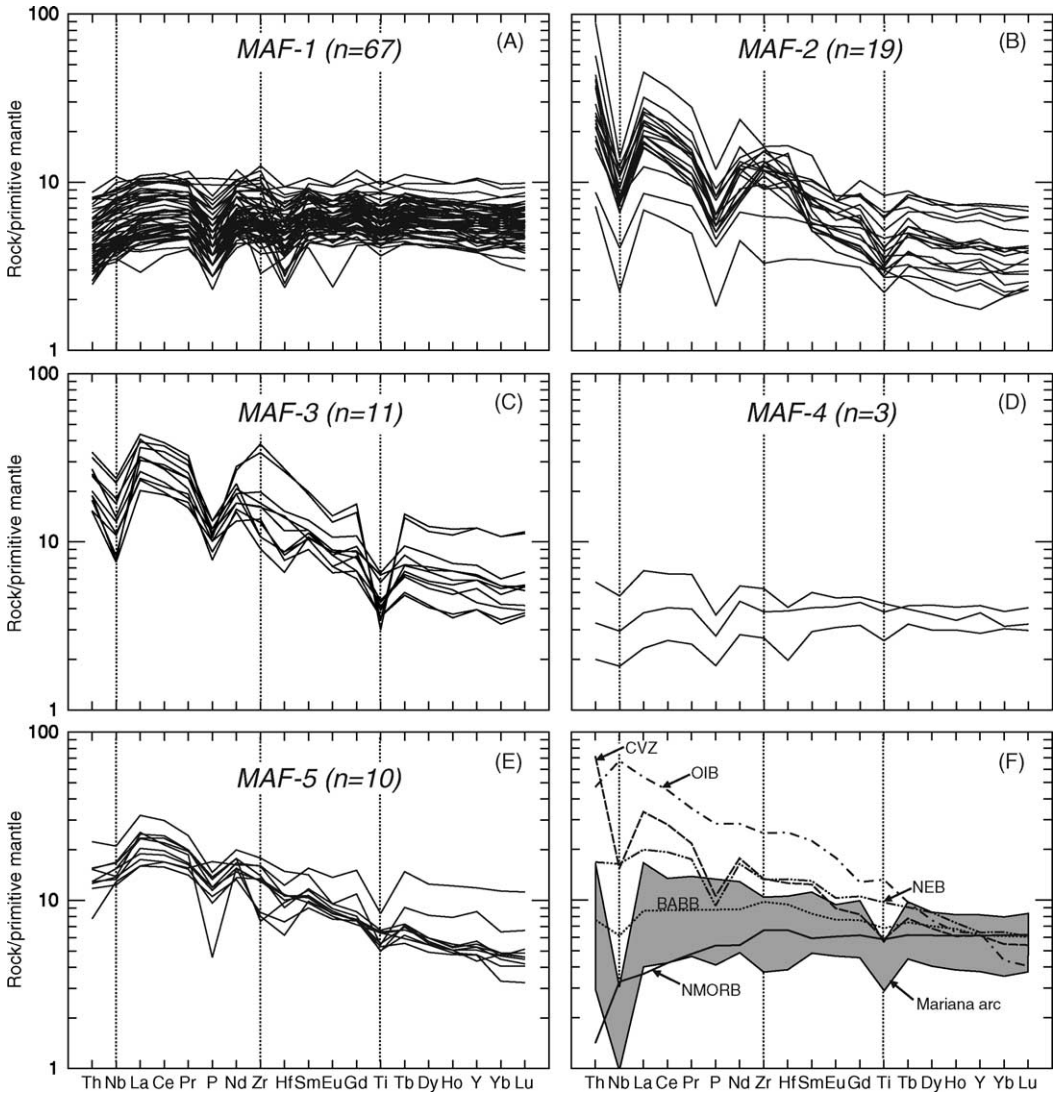

Fig. 8. (A–E) Primitive mantle normalized (Sun and McDonough, 1989) multielement plots showing the profiles for the five distinct groups of basaltic to andesitic rocks. (F) Shown for comparison are representative multielement profiles for NMORB and OIB (Sun and McDonough, 1989), a Nb-enriched basalt (NEB) from the Pickle Lake greenstone belt (PL95-27; Hollings, 2002), a basalt from the central volcanic zone of the Andes (CVZ; Sandeman, 1995), a bacK–Arc basin basalt (BABB) from the Scotia Sea (wx-47; Fretzdorff et al., 2002) and a field for 25 basalts from the Mariana arc (shaded field; Elliott et al., 1997). See text for further details.

by lower abundances of the incompatible elements, relative to the calc-alkaline rocks, although some tholeiitic samples exhibit elevated large ion lithophile (LIL) and light rare earth (LREE) elements. We further subdivide the basaltic to andesitic rocks into five distinct subgroups on the basis of their multielement patterns (Tables 1 and 2; Fig. 8A–E).

MAF-1 rocks predominate (occurring in both assemblage I and II), have relatively flat PM normalized profiles with slight depletions in Th, Nb and La relative to Ce and minor, variably developed negative Ti anomalies. Next in volumetric importance are the MAF-2 rocks (Tables 1 and 2), which exhibit variably fractionated multielement patterns having prominent

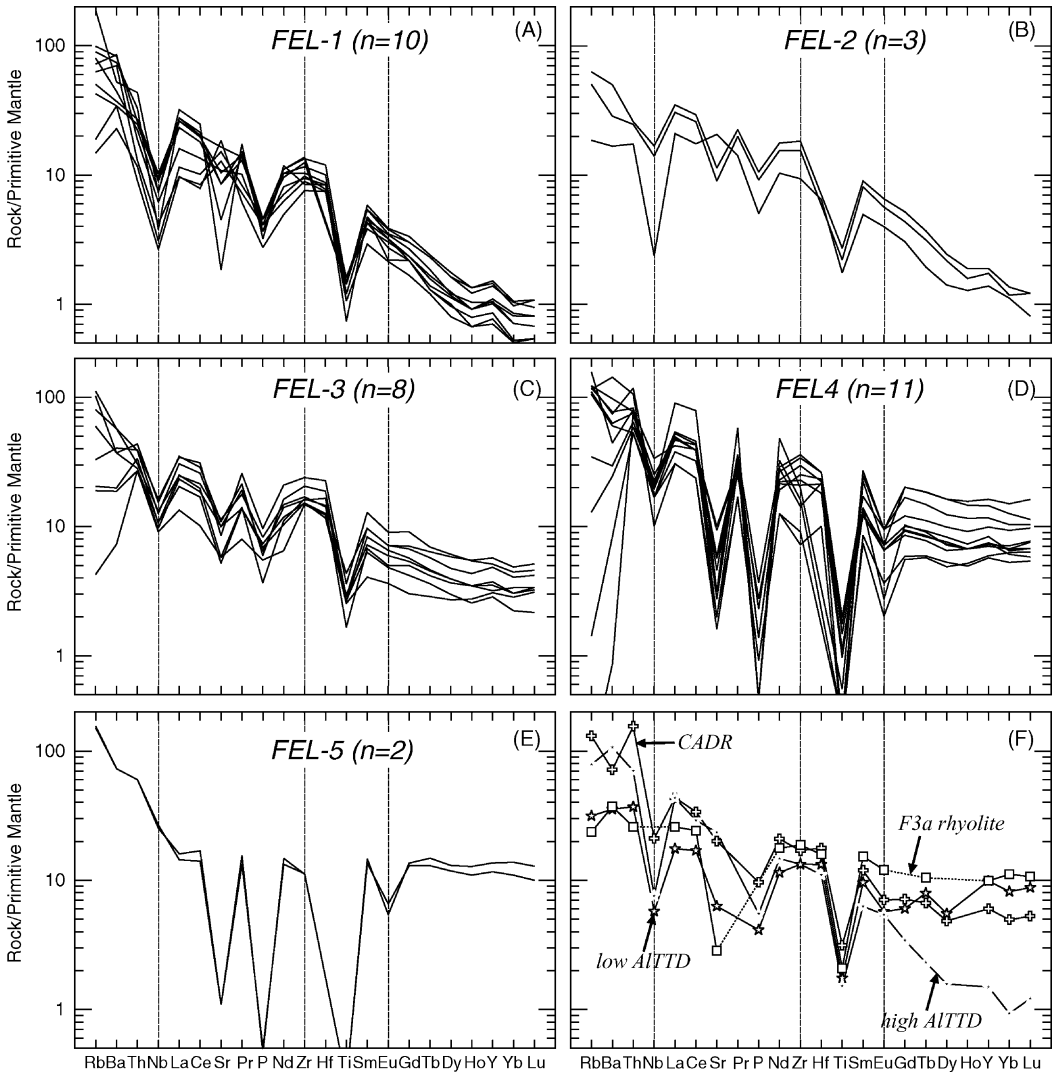

Fig. 9. (A–E) Primitive mantle normalized (Sun and McDonough, 1989) multielement plots showing the profiles for the five distinct subgroups of dacitic to rhyolitic rocks. (F) Shown for comparison are representative multielement profiles (from Drummond et al., 1996) for a high alumina tonalite–trondhjemite–dacite, a low alumina tonalite–trondhjemite–dacite, a calc-alkaline andesite–dacite–rhyolite and an FIIIa rhyolite from the Abitibi belt (Lesher et al., 1986). See text for details.

negative Nb and Ti anomalies relative to the REE and Th. Negative Eu anomalies are generally minor and variable. MAF-3 mafic units are less abundant (Tables 1 and 2), have fractionated multielement patterns and exhibit negative anomalies in Nb, Eu and Ti and, although similar to rocks of MAF-2, are characterized by chondrite-normalized Th/La (Th_N/La_N) < 1. MAF-4 mafic rocks are rare (Tables 1 and 2), have relatively flat PM normalized profiles with slight negative Nb and variable negative Ti anomalies and overall, low abundances of the incompatible elements. These are similarly characterized by Th_N/La_N < 1. MAF-5 rocks (Tables 1 and 2), have moderately fractionated multielement patterns that exhibit variable negative anomalies in Nb, Eu and Ti, and are also characterized by $Th_N/La_N \ll 1$. All of these groups occur in assemblage I whereas assemblage II lacks rocks of MAF-4.

Dacitic to rhyolitic rocks are also divided into five distinct subgroups by their multielement profiles, all of which are characterized by prominent negative HFSE anomalies (Fig. 9A–E; Tables 1 and 3). Assemblage II contains all of the felsic petrochemical subgroups outlined below, whereas assemblage I contains only petrochemical types FEL-1, -3 and -4. FEL-1 rocks (Tables 1 and 3) exhibit fractionated patterns and have slightly positive Y anomalies. FEL-2 felsic rocks are characterized by fractionated heavy rare earth element (HREE) depleted, multielement patterns and, distinctively, by $Th_N/La_N < 1$ (Tables 1 and 3). FEL-3 felsic rocks exhibit fractionated multielement patterns similar to those of FEL-1, but exhibit significantly less depletion in the HREE. FEL-4 rocks exhibit high abundances of the REE and LILE and negative Eu anomalies. These have less fractionated multielement patterns and, in particular, have elevated HREE abundances. FEL-5 felsic rocks are very rare and are confined to the volcanic apron of the arcuate, porphyritic domes exposed on the Cache Peninsula (Fig. 4). These exhibit unfractionated multielement profiles high Th and Nb relative to the LREE but have negligible negative Nb troughs. These rocks do, however, exhibit prominent negative P, Ti and Eu anomalies.

3.4. Nd isotopic data

For simplicity and ease of comparison, and because the total age span of the rocks erupted within the two volcanic assemblages is relatively small (ca. 35 Ma), all ϵNd values are recalculated to 2690 Ma (DePaolo, 1981; Table 4). Herein, we also incorporate the only previously published Nd data for rocks of the CHSB (Thériault and Tella, 1997). All specimens, including basaltic through rhyolitic rocks yield present day $^{144}Nd/^{143}Nd$ ratios ranging from 0.510990 to 0.513079, corresponding to $\epsilon Nd_{t=2690\,Ma}$ values of +0.3 to +3.5 (mean = +2.3; std. = 0.8; n = 23, Table 4). These data generally overlap, within error, the value for contemporaneous depleted mantle (DM), their mean value being identical to that for DM ($DM_{t=2690\,Ma}$ = +2.24; DePaolo, 1981) and the standard deviation comparable to the calculated analytical, 2σ standard deviation of 0.5. Four rocks, however, one each from MAF-2, 3 and 5 and FEL-4, have $\epsilon Nd_{t=2690\,Ma}$ between +1.2 and +0.3, generally lower than the remainder of the samples.

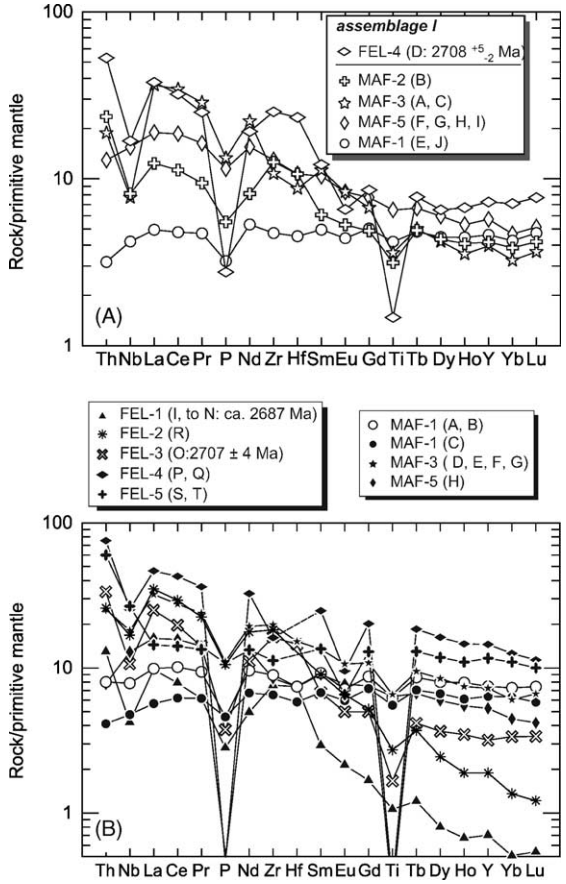

Fig. 10. (A) Primitive mantle normalized (Sun and McDonough, 1989) multielement plots showing the profiles for representative specimens from the Carr Lake locality. Note that the samples are coded to the locations on Fig. 3. (B) Primitive mantle normalized (Sun and McDonough, 1989) multielement plots showing the profiles for representative specimens collected from the Cache Peninsula locality. Note that the specimens are coded to the locations on Fig. 4. U–Pb ages (Patterson and Heaman, 1990; Davis et al., 2004) are given where known. Assemblage I are open symbols, assemblage II are filled symbols.

3.5. Geochemical variations in detailed localities

Multielement plots (Fig. 10A and B) are presented for selected specimens collected in the detailed localities outlined in Figs. 2–4 in order to underscore the areal and temporal distribution of the distinct geochemical subgroups at two sites for which we have age control.

The earliest recorded volcanism in the Kaminak segment for which sufficient petrochemical data is available is exposed along the eastern shore of Carr Lake

Table 4
Nd isotopic data for 23 volcanic rocks of the Kaminak segment including 17 for basaltic to andesitic units and 6 for felsic rocks

Sample	Volcanic group/type	Rock-type	Easting	Northing	Zone	Sm (ppm)	Nd (ppm)	$^{147}Sm/^{144}Nd$ measured	$^{143}Nd/^{144}Nd$ measured	2σ error	ϵNd_P	ϵNd_T
Mafic-intermediate												
HS420	1	PB	420354	6920430	15	2.59	7.69	0.2034	0.512906	1	5.2	2.9
HS426	1	PB	426288	6921856	15	2.51	7.48	0.2030	0.512926	6	5.6	3.4
HS423	1	PB	420053	6919739	15	22.07	74.06	0.1801	0.512455	4	−3.6	2.2
HS540	1	MB	422350	6933300	15	2.87	8.94	0.1944	0.512738	4	2.0	2.8
HS424	1	PB	420005	6919678	15	2.53	7.57	0.2018	0.512893	11	5.0	3.2
HS451	1	MB	405628	6909244	15	3.82	12.66	0.1827	0.512562	9	−1.5	3.4
HS421	2	PB	420382	6919897	15	18.34	82.65	0.1341	0.511633	13	−20.0	1.6
HS541	4	PB	422601	6933237	15	1.23	3.60	0.2064	0.512959	12	6.3	2.9
HS431A	1	PB	440097	6889487	15	2.49	7.47	0.2020	0.512890	10	4.9	3.1
HS517	1	PB	381047	6862084	15	2.92	9.10	0.1941	0.512694	9	1.1	2.0
HS530	1	PB	654858	6870928	14	2.16	6.36	0.2045	0.512884	11	4.8	2.1
HS432	1	PB	440358	6889404	15	2.51	7.46	0.2034	0.512904	9	5.2	2.9
HS444A	5	PBA	365059	6882865	15	4.42	18.93	0.1410	0.511758	9	−17.2	2.1
RR174B	3	PBA	418253	6916353	15	32.17	134.92	0.1441	0.511739	7	−17.5	0.7
HS445	5	PBA	365215	6882465	15	4.81	21.78	0.1334	0.511619	4	−19.9	2.1
HS433	5	PBA	439537	6880819	15	4.63	22.46	0.1246	0.511418	5	−23.8	1.2
HS435	2	PBA	439017	6880391	15	3.84	18.55	0.1251	0.511489	11	−22.4	2.4
Intermediate-felsic												
HS151	3	DAC	413288	6910029	15	15.16	74.77	0.1225	0.511474	5	−22.7	3.0
TP10A	1	RHY	410086	6912818	15	1.88	11.46	0.0989	0.510990	12	−32.1	1.7
HS92	4	RHY	349520	6884758	15	5.92	28.77	0.1243	0.511456	10	−23.1	2.0
HS057	4	RHYtuff	363447	6889448	15	5.33	26.22	0.1229	0.511465	6	−22.9	2.7
HS416A	4	RHY	392602	6908789	15	2.89	13.70	0.1277	0.511429	10	−23.6	0.3
HS527A	6	RHYbrecc	411355	6914893	15	5.87	16.58	0.2140	0.513079	10	8.6	2.6

Key: ϵNd_P, present day value; ϵNd_t, calculated to t = 2690 Ma; PB, pillowed basalt; MB, massive basalt; PBA, pillowed basaltic andesite; DAC, dacite; RHY, rhyolite; RHYtuff, rhyolite tuff; RHYbrecc, rhyolite breccia; utm coordinates in NAD 27 projection.

(Fig. 3) and comprises a sequence of intercalated rhyolitic tuffs and massive to amygdaloidal, calc-alkaline basaltic andesite flows or fine-grained tuffs. The rhyolitic tuff (FEL-4) is LREE enriched (Fig. 10A), with classic, arc-like negative Nb, P, Ti anomalies but a relatively flat HREE profile. The mafic rocks exposed adjacent to the felsic tuff belong to MAF-2 and 3, have calc-alkaline arc-like characteristics including LIL and LREE-enrichment (Fig. 10), and negative Nb, P and Ti anomalies. MAF-2 rocks, however, exhibit Th_N/La_N >1 and positive Zr and Hf anomalies in contradistinction to rocks of MAF-3. Basalts and basaltic andesites exposed ca. 4 km farther south (Fig. 3) appear to represent an interlayered series of two geochemically distinct groups. The northern and southern parts of the pillowed sequence are dominated by tholeiitic pillow basalts with flat to slightly LREE depleted multielement profiles (MAF-1).The central portion of the southern section is underlain by pillowed and massive transitional calc-alkaline basalts having convex-upwards multielement profiles typical of MAF-5 mafic units.

On the Cache peninsula, the oldest felsic volcanic unit (2707 ± 4 Ma; Davis et al., 2004) is a FEL-3 rock exhibiting arc-like geochemical characteristics but having only a moderately fractionated multielement profile (O; Figs. 4 and 10B). The relative ages of the majority of the mafic volcanic rocks is poorly constrained but on the basis of field relationships they are interpreted to be younger than this felsic unit. Thus, with the exception of some MAF-1 rocks, most mafic volcanic rocks belong to assemblage II. Assemblage II mafic rocks exposed on the peninsula comprise tholeiitic pillow basalts with essentially flat to slightly LREE depleted multielement profiles (MAF-1); rare basaltic andesites with moderately fractionated multielement patterns that exhibit variable negative anomalies in Nb, Eu and Ti, and are also characterized by $Th_N/La_N \ll 1$

(MAF-5) and basaltic to andesitic lavas having fractionated multielement patterns with negative anomalies in Nb, Eu, Ti and having $Th_N/La_N < 1$ (MAF-3). The younger felsic rocks exposed on the peninsula comprise examples of FEL-1, 2, 4 and 5 (Figs. 4 and 10B).

4. Discussion

A number of features of the volcanic rocks of the Kaminak segment and the CHSB as a whole (see Cousens et al., in press) are incompatible with standard models for Archaean greenstone belts (see Tomlinson and Condie, 2001). The presence of extensive juvenile tholeiitic basalts implies that the CHSB most closely resembles Tomlinson and Condie's "Platform model". However, the following observations indicate that such a model does not adequately explain the features of the CHSB: (1) widespread, felsic lavas and tuffs are common throughout the entire temporal evolution of the supracrustal belt but increase in volume in assemblage II; (2) ultramafic and high-MgO volcanic units are very rare, confined to one known locality (S. Barham, Comaplex Minerals Corp., personal communication 2001); (3) chemical and clastic metasedimentary rocks appear to occur throughout the stratigraphic sequence; (4) four of the five geochemical groups of basaltic to andesitic volcanic rocks, including MAF-1, 2, 3 and 5, occur interlayered throughout the stratigraphy of both assemblages (MAF-4 is absent in assemblage II).

Furthermore, the following observations would appear to be incompatible with a classical volcanic arc, localized on normal oceanic MORB crust above a subduction zone (see also Hanmer et al., in press); (5) although prominent felsic volcanic edifices are developed throughout the stratigraphy, only those of assemblage II are accompanied by voluminous intermediate to felsic plutons; (6) felsic centres of assemblage II did not coalesce to form a prominent volcanic arc, but may represent an "incipient" arc; (7) contemporaneous arc-like signatures are distributed across the entire Hearne domain (Davis et al., 2000; Sandeman et al., 2000, 2001), equivalent to a swath ~225 km wide, without lateral temporal polarity one might expect from a migrating arc-system. This is an order of magnitude greater than the widths of more recent, localized arcs; (8) supracrustal stratigraphic units appear to have developed in laterally discontinuous basins, possibly delimited by extensional faults and; (9) broken formations, typical of accretionary wedges, are lacking.

In view of these observations, none of the current models for Archean greenstone belt development appear to adequately explain the geological development of the CHSB. A suitable model must offer an explanation for the simultaneous emplacement of basaltic to andesitic magmas, characterized by diverse geotectonic affinities, and intercalation of similarly, compositionally diverse felsic volcanic rocks. In light of these observations, we discuss the lithogeochemical and Nd isotopic characteristics of the volcanic rocks in order to evaluate their petrogenesis and formulate a plausible geodynamic model for the region.

4.1. Petrogenesis of basalts to andesites

Basaltic to andesitic volcanic rocks of the Kaminak segment consist of abundant tholeiitic and less common calc-alkaline rocks. These were erupted in two volcanic assemblages, each of which contains a number of contemporaneous geochemical subgroups (Figs. 8 and 9; Table 1). The tholeiitic basalts exhibit FeO^T and TiO_2 enrichment trends with increasing fractionation, but have compatible element abundances inconsistent with them being derived from peridotitic mantle. Irrespective of their stratigraphic assemblage, lithogeochemical variations of the tholeiitic rocks imply fractionation of an assemblage including olivine + clinopyroxene, whereas depletion of the elements Eu and Sr suggests minor effects of plagioclase fractionation. Calc-alkaline rocks of both assemblages, however, exhibit scattered inter-element variations, a feature incompatible with them being related through simple petrogenetic processes. Their Ti, Y, Nb, Zr interrelationships imply that other mineral phases, possibly hornblende, magnetite or biotite, were fractionated from the calc-alkaline primary melts.

Primitive mantle normalized multielement plots (Sun and McDonough, 1989; Fig. 8A–E), clearly outline five distinct subgroups within the mafic rocks of both volcanic assemblages of the CHSB. These are compared to representative mafic volcanic rocks from a variety of tectonomagmatic settings (Fig. 8F). Greatly dominant, tholeiitic MORB-like basalts and rare basaltic andesites of MAF-1 exhibit variable patterns with mild LILE and LREE enrichment and depletion that generally lack Nb troughs, but have variable

Hf and Zr anomalies. These rocks are the dominant mafic geochemical rock-type throughout the belt and, although they exhibit less depletion of the LREE, Th and Nb, these may represent the Archaean analogue of modern MORB (Archaean mid ocean ridge basalts; Fig. 8F) (cf. Ohta et al., 1996). MAF-1 rocks form a large proportion of assemblage I and a lesser component of assemblage II. MAF-2 rocks comprise rare basalts and predominant basaltic andesites to andesites that are calc-alkaline, have elevated Th and LREE, show variable HFSE troughs, and closely resemble volcanic arc mafic rocks of modern oceanic and continental margins (Fig. 8F; Pearce, 1982; Elliott et al., 1997). These occur throughout the stratigraphy but are more abundant in assemblage II. MAF-4 rocks comprise rare tholeiitic basalts that are restricted to volcanic assemblage I. They have low abundances of the incompatible elements, exhibit minor LREE enrichment or depletion, have small negative Nb anomalies and most closely resemble modern back–Arc basin basalts (BABB; Fig. 8F). These are considered to be generated through melting of strongly depleted asthenosphere but with a minor crustal input, typically by contamination of their mantle source via subduction (Saunders and Tarney, 1991; Hawkins, 1995). MAF-5 rocks comprise transitional calc-alkaline basalts through andesites with elevated LREE, Nb_N/La_N = 0.6–0.8, Zr/Y = 3.3–8.3, and low Th_N/La_N but high La_N/Nb_N. These features, particularly their convex-upwards multielement patterns, demonstrate that these are most similar (Fig. 8F) to OIB-like, Nb-enriched basalts (NEB; Sajona et al., 1996; Hollings and Kerrich, 2000; Wyman et al., 2000; Hollings, 2002). Recent models for the genesis of NEB's suggest that many of these, notably those associated with high alumina tonalite–trondhjemite–granite (TTG) suites in the Archaean (e.g., Martin, 1987, 1999), could have formed in subduction environments where their mantle sources were metasomatically modified through the introduction of adakitic slab-melts (Lafleche et al., 1992; Sajona et al., 1996; Hollings and Kerrich, 2000; Wyman et al., 2000, 2002; Hollings, 2002). Subsequent melting of the melt-modified mantle, at depths within the garnet stability field, yield LREE- and Nb-enriched and variably HREE depleted NEB melts. MAF-3 calc-alkaline basalts to andesites occur in both assemblages, are similar to those of MAF-2 in having elevated LREE and HFSE troughs, but are characterized by low Th_N/La_N values (Fig. 8C). The latter feature is common in continental- or arc-rift basalts (Barrie et al., 1993; Dostal and Mueller, 1997; Gribble et al., 1998) and is inferred to arise through crustal contamination of primary mantle melts (Fig. 8F). The multielement patterns for the MAF-3 rocks may be reproduced through two plausible processes. Hypothetical mixing of ca. 75–90% OIB-like (MAF-5) and ca. 10–25% of arc-like (MAF-2) melts yields multielement profiles comparable to those for the MAF-3 rocks. Alternatively, assimilation and fractional crystallization (AFC) by MAF-5 magmas of LILE- and LREE-enriched crust with HFSE anomalies, and similar overall to the majority of the Neoarchaean granitoids of the region, can also reproduce the multielement profiles of the MAF-3 rocks. Discriminating between these two processes, however, is difficult. This type of Th–Nb–La inter-element behavior appears to be a common, but rarely addressed phenomenon in basaltic rocks of Archaean greenstone belts (Dostal and Mueller, 1997; Polat et al., 1998; Tomlinson et al., 1998, 1999; Wyman et al., 1999) and has been attributed to reflect crustal contamination during the incipient rifting of pre-existing mafic (oceanic?) crust.

A common feature of many of the basaltic rocks of the region, in particular the transitional to calc alkaline rocks of MAF-2, 3 and 4, are variable negative and positive Zr (Hf) anomalies in their multielement patterns. Minor negative anomalies in basaltic rocks are readily attributed to fractionation of a Zr-bearing phase such as hornblende or magnetite (Rollinson, 1993; Hollings and Kerrich, 2000), whereas positive Zr (Hf) anomalies have been attributed to the incompatibility of Zr in residual amphibole during partial melting in the garnet stability field (Pearce and Peate, 1995; Drummond et al., 1996). Wolde et al. (1996) alternatively suggested that the low Zr/Sm ratios in observed in boninitic rocks of southern Ethiopia likely resulted from partial melting of an orthopyroxene-rich, but clinopyroxene-poor mantle source.

To further elaborate on the sources of the mafic rocks, we present in Fig. 11 plots of log Th/Yb versus log Ta/Yb (after Pearce, 1982) and La_N/Sm_N versus Th/Nb (after Elliott et al., 1997). The incompatible element ratios Ta/Yb and La_N/Sm_N are useful in discriminating levels of incompatible element enrichment of plausible mantle sources whereas variation in the ratios Th/Yb and Th/Nb outline differences in

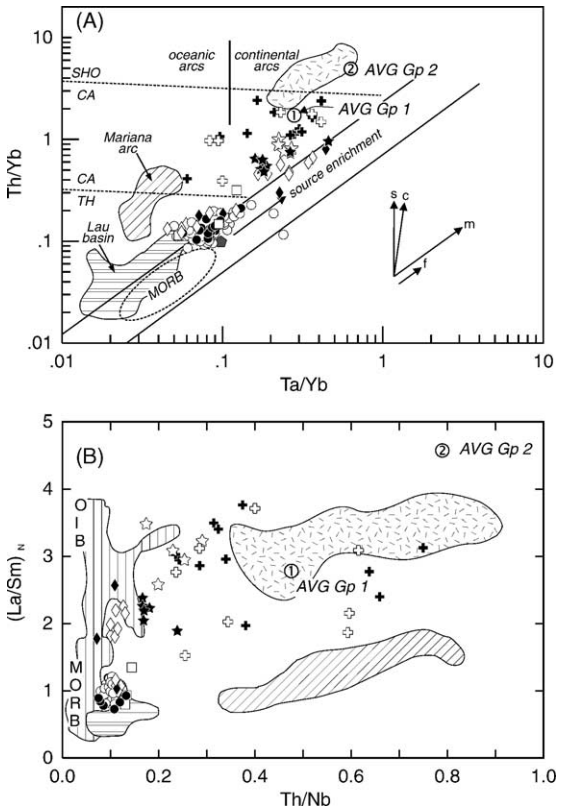

Fig. 11. Incompatible element ratio plots for volcanic rocks of the CHSB. (A) A plot of Th/Yb vs. Ta/Yb (after Pearce, 1982) for basaltic to andesitic rocks demonstrating their variability in Th/Yb relative to the mantle array. Note that the MAF-2 rocks are characterized by high Th/Yb, some being comparable to volcanic rocks of modern continental arcs. Symbols as in Fig. 5. *Key:* shaded pentagon is primordial mantle; circle with number 1, the mean composition of 34 Group 1 granitoids from the Kaminak segment (Sandeman et al., 2004); circle with number 2, the mean composition of 63 Group 2 granitoids from the Kaminak segment (Sandeman et al., 2004); diagonally ruled field, Mariana Arc data (Elliott et al., 1997); horizontally ruled field, Lau Basin data (Pearce et al., 1995); stippled field, data for 21 calc-alkaline to shoshonitic basalts from the central volcanic zone of the Andes (Sandeman, 1995). Labeled trajectories represent: s, subduction; c, crustal contamination; m, mantle source variation; f, ca. 50% fractional crystallization of olivine + clinopyroxene + plagioclase. (B) A plot of La_N/Sm_N vs. Th/Nb (after Elliott et al., 1997) for mafic to intermediate volcanic rocks of the Kaminak segment demonstrating their variability in Th/Nb relative to the mantle array (vertically ruled field). Symbols as in Figs. 5 and 11A.

the amount of crustal input into the magmas. These diagrams demonstrate that MAF-1 rocks, although mildly enriched in Th and Ta, are closely analogous to modern MORB-like basalts. All of the MAF-2 rocks plot above the mantle array in Fig. 11A the majority having incompatible element ratios similar to volcanic rocks of continental arcs (cf. Pearce, 1982). These have variable, but high values for all four element ratios, overlapping with or greater than those characterizing the intra-oceanic Mariana Arc (Elliott et al., 1997). Rocks of MAF-3 have variable, but generally higher Ta, Th and La, and thus represent LREE-enriched melts that exhibit evidence of crustal contamination. It is unclear at this time if the contamination occurred in the mantle source (i.e., subduction-related) or during ascent through the crust. MAF-4 rocks are mildly enriched in Th and Ta relative to MAF-1 rocks, plotting close to the field for the Lau Basin (Pearce et al., 1995), suggesting that they are likely BAB-like basalts. MAF-5 rocks exhibit Ta/Yb, Th/Yb and La_N/Sm_N values most compatible with OIB-like basalts as they fall in the Ta/Yb-enriched part of the mantle array on Fig. 11A and exhibit high La_N/Sm_N approaching those for OIB (Fig. 11B). We note that although these can be described as Nb-enriched basalts (see above), their distinct incompatible element abundances and variations may reflect their derivation from an OIB-like mantle component rather than from partial melting of sub-arc mantle that has been modified by infiltration of adakitic melts. These data suggest therefore, that two distinct mantle sources were probably involved in the petrogenesis of the volcanic rocks, and that the rocks of MAF-2, 3 and to a lesser extent MAF-4, may have been contaminated with Th- and Ta-enriched crustal material.

4.2. Petrogenesis of dacites and rhyolites

Dacitic to rhyolitic volcanic rocks from both assemblages of the Kaminak segment exhibit calc-alkaline affinities. The felsic units, irrespective of their stratigraphic setting, are characterized by non-systematic variation of most elements with increasing SiO_2 suggesting that they are not linked through simple petrogenetic processes.

The felsic rocks comprise five distinct subgroups on the basis of their primitive mantle-normalized, multi-element patterns (Fig. 9A–E; Table 1). FEL-1 and 2 are characterized by strongly fractionated profiles with HREE depletion, variably developed negative Nb, P and Ti anomalies and, an absence of Eu troughs. All of these points indicate that FEL-1 and 2 felsic rocks are most similar to high-alumina TTG rocks (Fig. 9F)

and were probably generated through partial melting of a garnet-bearing, basaltic source, either an eclogitic, down going slab (cf. Drummond and Defant, 1990; Martin, 1999) or possibly garnetiferous, mafic lower crust (Smithies, 2000; Kamber et al., 2002). FEL-3 rocks exhibit similar multielement profiles to those of FEL-1 and 2, however, HREE are more abundant and they have modest negative Eu anomalies indicating a minor amount of plagioclase fractionation. Overall these FEL-3 rocks have compositions comparable to low-alumina TTG or possibly calc-alkaline andesite–dacite rhyolite (CADR) suites of magmatic arcs (Fig. 9F). Their multielement patterns suggest an absence of, or a lower proportion of garnet in their source and hence, a shallower depth of generation. These rocks exhibit in the crust. FEL-4 rocks are more strongly enriched in all of the incompatible elements, have pronounced negative Nb, P and Ti anomalies, flat HREE profiles, but well-developed negative Eu anomalies. These are similar to CADR and exhibit (Fig. 9F) features that imply they formed through partial melting of intermediate (?) crust in the absence of garnet, and that the magmas underwent significant fractionation of plagioclase in upper crustal magma chambers. FEL-5 rocks are comparable in most aspects, with the exception of higher Th, to the classic FIIIa rhyolites of the Abitibi Belt of the Superior Province (Fig. 9F; Lesher et al., 1986). These exhibit flat multielement profiles with enrichments in Th and Nb, but prominent negative P, Eu and Ti troughs. These are interpreted to have formed through plagioclase dominated, extensive fractional crystallization of mafic precursors in high-level crustal magma chambers.

In Fig. 12A and B, we attempt to elaborate on the processes and sources involved in the genesis of the felsic volcanic rocks of the Kaminak segment. Fig. 12A displays the primitive mantle normalized REE patterns for representative specimens of the five felsic volcanic subgroups and compares them to fields defined by 10 and 25% model melts from a number of mafic crustal sources (Table 5). Assuming batch melting and appropriate partition coefficients (Table 5; Martin, 1987) the REE patterns of the FEL-1 and -2 rocks closely match the slopes of melts derived from eclogite and garnet-bearing (25%) amphibolite, respectively. Similarly, the REE pattern for the FEL-3 rock closely matches the slopes of melts generated from batch melting of amphibolite and amphibolite with 10% garnet. The REE

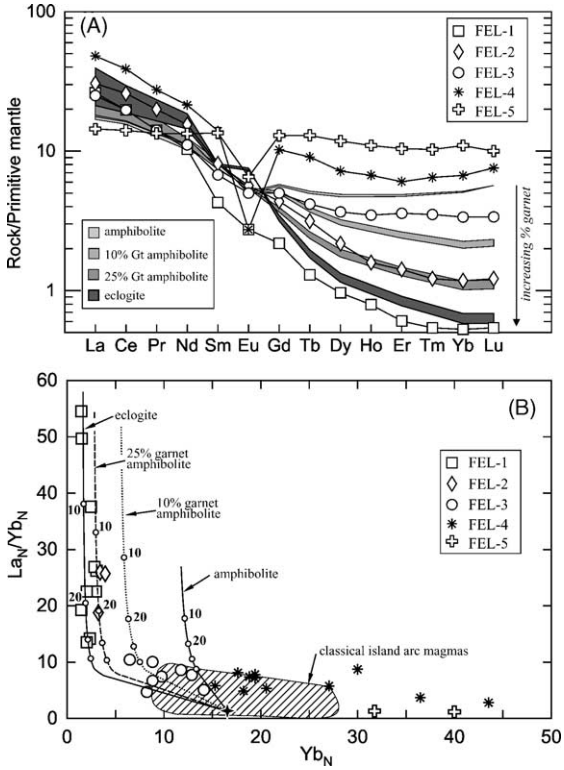

Fig. 12. (A) Primitive mantle normalized REE patterns for representative samples from each of the five felsic subgroups. These are compared to fields defined by 10 and 25% batch melting of average Kaminak segment, MAF-1 mafic volcanic rock. The calculated patterns for the batch melting are for potential protoliths comprising amphibolite, 10% garnet amphibolite, 25% garnet amphibolite and eclogite residues (see Table 5; modelled after Martin, 1987; Drummond and Defant, 1990). (B) La_N/Yb_N vs. Yb_N plot for the felsic volcanic rocks. Diagonally ruled field is for classical island arc magmas that evolve via fractional crystallization (from Drummond and Defant, 1990). Equilibrium melting curves for an average MAF-1 composition (Table 5) are shown with amphibolitic, garnet amphibolitic and eclogitic mineral residues. Labeled white dots indicate 10% increments of melting. Note that all FEL-4 and -5 samples fall to the right of the melting curves and appear to have evolved via fractional crystallization.

patterns for FEL-4 and -5 rocks do not match those for partial melts of mafic crustal sources. Fig. 12B outlines the distinctive REE compositions of the felsic volcanic rocks of the region in terms of their chondrite normalized La_N/Yb_N and Yb_N values. Here, we show melting curves for an average composition for the most abundant mafic rocks (MAF-1) of the Kaminak segment (Table 5) with amphibolite, garnet (10%) amphibolite,

Table 5
Starting compositions and partition coefficients used in batch melting calculations

Sample	Average MAF-1 mafic rock (ppm)	Clinopyroxene (cpx)	Hornblende (hbl)	Plagioclase (plag)	Garnet (gar)
La	4.41	0.1	0.2	0.13	0.04
Ce	11.87	0.2	0.3	0.11	0.08
Nd	9.27	0.4	0.8	0.07	0.20
Sm	2.95	0.6	1.1	0.05	1.00
Eu	1.03	0.6	1.3	1.30	0.98
Gd	4.00	0.7	1.8	0.04	3.8
Tb	0.70	0.7	2.0	0.037	7.5
Dy	4.54	0.7	2.0	0.031	11.0
Er	2.83	0.6	1.9	0.026	16.0
Yb	2.82	0.6	1.7	0.024	21.0
Lu	0.42	0.6	1.5	0.023	21.0

Note: Melting model residues: eclogite = 50% cpx + 50% gar; 25% garnet amphibolite = 10% cpx + 25% gar + 50% hbl + 15% plag; 10% garnet amphibolite = 15% cpx + 10% gar + 50% hbl + 25% plag; amphibolite = 5% cpx + 30% plag + 65% hbl. Partition coefficients are from Martin (1987).

garnet (25%) amphibolite and eclogite residual mineral assemblages. Partial melting of eclogite or garnet-bearing residual amphibolite assemblages can readily produce the spectrum of compositions exhibited by the FEL-1 and -2 rocks, and melt compositions comparable to the FEL-3 rocks can be generated through higher degrees of partial melting of weakly garnetiferous sources. Rocks of FEL-4 and -5, however, are not melts of mafic crust and likely represent fractionates of mafic progenitors.

4.3. Implications of Nd isotopic data

Nd isotopic determinations indicate that the tholeiitic samples exhibit on average slightly higher ϵNd values and corresponding lower SiO_2 contents relative to the calc-alkaline rocks. In Fig. 13, we have plotted ϵNd_t versus chondrite normalized Th_N/Nb_N, a value that acts as a proxy for the extent of crustal contamination in mantle-derived rocks. Therein, the ϵNd_t and Th_N/Nb_N values for three of the five distinct subgroups of basaltic to andesitic rocks (12 MAF-1, 4 MAF-5 and 1 MAF-4 basalts; Tables 1 and 3; Fig. 12) form a tight cluster and overlap, within error. One sample each of a MAF-2 and MAF-3 basalts have Th_N/Nb_N comparable to the main cluster, but exhibit lower ϵNd_t values. Two other mafic samples, one of MAF-2 and one of MAF-3, overlap within error the ϵNd_t values of the main cluster, but exhibit higher Th_N/Nb_N. All six of the dacitic to rhyolitic samples along with two specimens of MAF-2 basalts are characterized by variable ϵNd_t but elevated Th_N/Nb_N relative to the main cluster. These data indicate that although the spread of data to the right of the mantle array may be a result of contamination by Th-enriched crustal material (Kaminak segment granitoids?), at least four specimens exhibit ϵNd_t and Th_N/Nb_N variations that cannot be easily produced via this model. Instead, it appears that these variations must have arisen through differences in their mantle source (i.e. melting of MORB-like versus OIB-like sources) and/or through contamination via introduction of $^{143}Nd/^{144}Nd$ depleted and LREE- and LIL-enriched, significantly older crustal material.

In discussing the U–Pb geochronology of the CHSB, Davis et al. (2004) demonstrate that of 26 U–Pb ages obtained in the region, inheritance of zircon from crust older than ca. 2710 Ma is lacking. Moreover, $\epsilon Nd_{t=2690\,Ma}$ values for 15 plutonic rocks from the CHSB range from +1.1 to +3.2 (mean = +2.2), overlapping, within error, with the value for depleted mantle of the time (see Sandeman et al., 2004). Because the ϵNd values for all of the volcanic rocks range from +0.7 to +3.5 (mean = +2.4), we suggest that extensive contamination via assimilation of significantly older continental crust is unlikely. We suggest that because the crust of the Kaminak segment appears to have formed rapidly (ca. 2666–2711 Ma), and comprises juvenile material with Nd isotopic characteristics identical, within error, to contemporaneous depleted mantle, the most viable means of generating these features is through the introduction of detritus into an active subduction zone. Hence, the contrasting

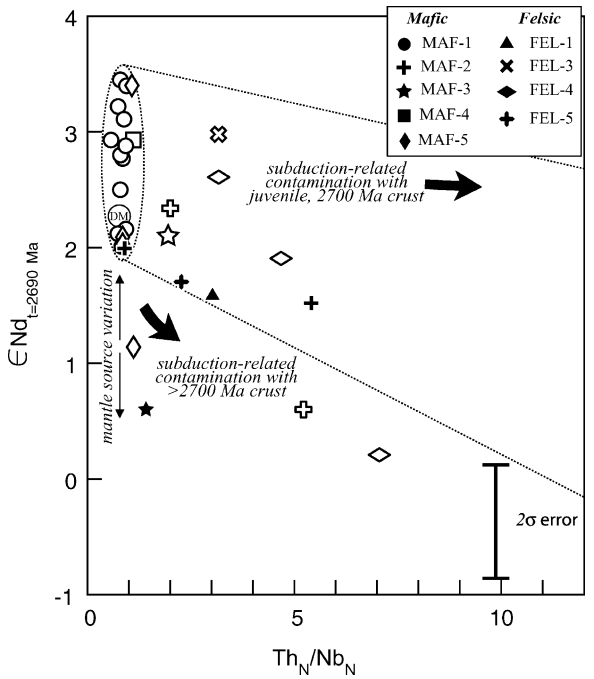

Fig. 13. $\varepsilon Nd_{t=2690\,Ma}$ vs. primitive mantle normalized Th_N/Nb_N (Sun and McDonough, 1989) for 29 specimens from the Kaminak and Tavani segments of the CHSB (this study; Thériault and Tella, 1997), including those from volcanic assemblage I (open symbols) and assemblage II (filled symbols). Depleted mantle or MORB melts are represented by the circle with the DM. Mantle source variations are represented by the labeled vertical arrows. An envelope and trajectory arrow are shown to demonstrate the effects of contamination of mafic rocks with juvenile, ca. 2700 Ma felsic crust. Also shown is a trajectory arrow showing the effect contamination of the mantle sources with older, more evolved continental crust. ϵ_{Nd} results are calculated at 2690 Ma and the parameters for the calculation of ϵNd include: $^{143}Nd/^{144}Nd_{0(CHUR)} = 0.512638$; $^{147}Sm/^{144}Nd_{(CHUR)} = 0.1967$ (Jacobsen and Wasserburg, 1980). The depleted mantle curve was calculated according to the parameters of DePaolo (1981).

trace element signatures of the five geochemically defined basaltic to andesitic subgroups are more likely derived from geochemically distinct, but isotopically similar (Nd) mantle sources. If crustal contamination has played a role in the genesis of these rocks, then it must have been minor, and/or predominantly involved isotopically young, juvenile Neoarchaean crust isotopically similar to the volcanic units.

The minor isotopic variability and high Th_N/Nb_N observed in a proportion of the mafic and felsic volcanic rocks of the CHSB can be in part attributed to the assimilation of juvenile ca. 2700 Ma crust during ascent or alternatively, particularly for the mafic rocks, contamination of their mantle sources via subduction-modification (Fig. 13). This process does not, however, account for the low ϵNd values and elevated Th_N/Nb_N values displayed by three mafic rocks belonging to MAF-2, -3 and -5 (and one specimen of FEL-4). Instead, it appears that these rocks derived their LIL and LREE enrichment along with their less radiogenic Nd isotopic compositions through addition of small amounts of older crustal material to their mantle source via subduction.

4.4. Conclusions

Volcanic rocks of the Kaminak segment of the CHSB range in age from 2681 to 2711 Ma (Davis et al., 2004), and comprise two volcanic assemblages designated on the basis of their lithological associations, U–Pb (TIMS; zircon) ages, spatial distribution and petrological characteristics. Nd isotopic data indicates that, although minor contamination by older, more evolved crustal sources may be required, the vast majority of the volcanic rocks of the region are juvenile and were recently removed from depleted mantle at their time of crystallization. In Fig. 14, we present lithogeochemical data for rocks from a number of localities within both assemblages, and place these within their respective stratigraphic setting. Assemblage I comprises a sequence of pillowed and massive basalts intercalated on the outcrop-scale with sparsely distributed dacitic to rhyolitic flows and rare chemical and clastic metasedimentary rocks, collectively inferred to represent an extensive, predominantly mafic subaqueous platform. These rocks comprise three distinct subgroups of felsic rocks and all five subgroups of mafic rocks. Broadly contemporaneous gabbroic through granodioritic plutonic rocks (Central Kaminak Intrusive Suite; Fig. 14) intrude this sequence. Assemblage I was deformed at ca. 2686–2690 Ma, generating upright foliations and steeply dipping bedding.

Concomitant and subsequent to this deformation event (Hanmer et al., in press; Davis et al., 2004) assemblage II volcanic rocks were emplaced on top of the assemblage I. Assemblage II comprises predominant andesitic to dacitic volcaniclastic rocks with less abundant basaltic and rhyolitic end members that are considered to have formed a series of spaced, central volcanic edifices. These rocks comprise five distinct

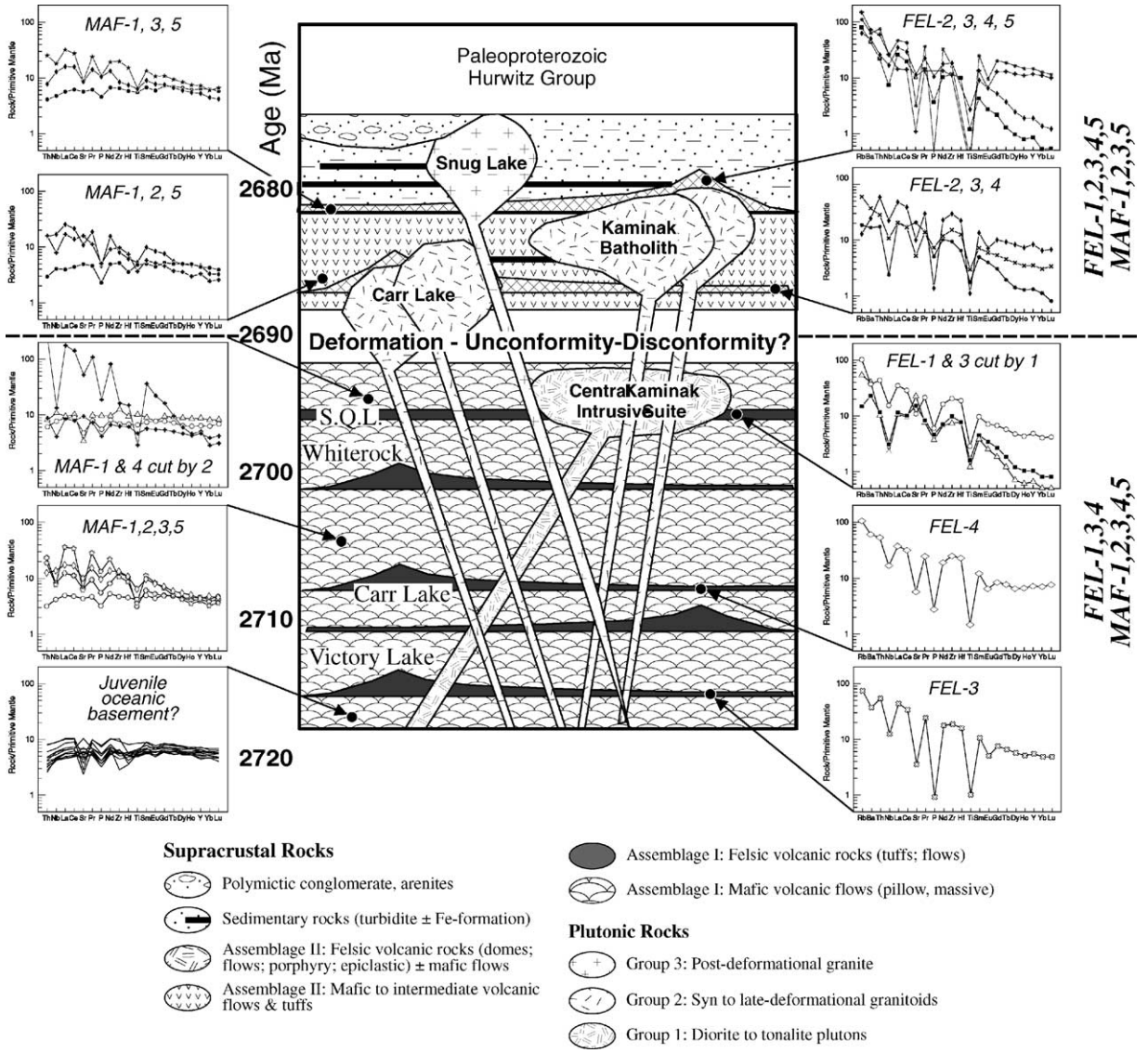

Fig. 14. Schematic stratigraphic section for rocks of the Kaminak and Tavani segments with the locations of critical localities for which we have obtained field, U–Pb geochronological and lithogeochemical data. Note that assemblage I is characterized by rocks belonging to all five mafic, and three of five felsic subgroups. Similarly, assemblage II contains four of five mafic and all five felsic subgroups.

subgroups of felsic rocks and four of five subgroups of mafic rocks. Accompanying and postdating volcanic assemblage II, a voluminous series of gabbroic through granitic plutons (Group 2 plutons; Sandeman et al., 2004) were intruded, disrupting and exerting significant influence on the distribution of the pre-existing, discontinuous volcanic stratigraphy and hence heralding a major change in the tectono-magmatic setting. The complete stratigraphy was then cut by late, post-tectonic monzogranite and rare alkaline intrusions.

The near absence of plume-related komatiites throughout, and the presence of arc-like MAF-2 rocks in both assemblages, supports a subduction-related origin for all of the volcanic rocks of the CHSB. Moreover, the abundance of mafic rocks, particularly of MAF-1,

but also those of all other subgroups, collectively implies that the mantle yielding the mafic-intermediate volcanic rocks of both assemblages was heterogeneous on a reasonably small-scale. Rocks of the MAF-5 subgroup, described as consisting of OIB-like or NEB-like rocks do not require the presence of a mantle plume. These rocks indicate instead that either pockets of an OIB-like mantle source were dispersed throughout the asthenospheric mantle of the CHSB, or alternatively, the sub-CHSB asthenosphere may have experienced metasomatic modification by adakitic, slab-derived melts, thereby yielding NEB-like rocks during partial melting (Hollings and Kerrich, 2000; Wyman et al., 2000; Hollings, 2002). Unlike those authors, however, on the basis of our field, geochronological and petrochemical observations we do not appeal to a back–Arc tectonomagmatic setting for formation of the CHSB.

In contrast, the lithospheric-scale processes involved in the extensional "infant arc" scenario appear to be more compatible with the geology of the CHSB, and in particular the petrologically diverse, contemporaneous, juvenile volcanic rocks of assemblage I. The extensional "infant arc" scenario was originally formulated to account for the development of broad (100s km) swaths of oceanic crust adjacent to subsiding slabs in the Eocene proto-arcs of the SW Pacific Ocean, prior to the localization of classical volcanic arcs above subduction zones (Stern and Bloomer, 1992; Bloomer et al., 1995; Wyman et al., 1999). According to this model, near-vertical, gravity-driven subsidence of a lower plate is accompanied by rapid hinge retreat that induces extension of the upper plate and convective flow in the underlying lithospheric and asthenospheric mantle. Adiabatic decompression in the upwelling mantle, together with transfer of LILE-charged water (and silicate melts?), and from the subsiding crust to the overlying mantle wedge, lead to melting and eruption rates four to five times greater than those of modern arcs, but comparable with slow spreading ridges (*"pre-arc spreading"* of Pearce et al., 1984). In only 10 m.y., this magmatism can generate an extensive (200–400 km wide) swath of juvenile crust that is much broader than localised, active arc systems (35–50 km, or less). In our companion paper (Hanmer et al., in press), we have suggested that the geological characteristics of the CHSB, briefly listed above, are compatible with this model.

An absence of low-Ti rocks in the CHSB may be taken as problematic for application of this model. We propose, however, that their absence in the Kaminak segment of the CHSB may reflect our poor understanding of the geochemical mass balance of Neoarchaean asthenospheric mantle (see Francis, 2003). If one assumes that substantial amounts of continental crust may not have been extracted from the Neoarchaean mantle by ca. 2700 Ma, then it is likely the asthenosphere at that time was less depleted than the present. Thus, mafic rocks similar to the voluminous MAF-1 subgroup in the Kaminak segment and also prominent in many greenstone belts of similar age worldwide (cf. Tomlinson et al., 1998, 1999, 2002; Polat et al., 1998; Hollings et al., 1999; Cousens, 2000; Hollings, 2002), may represent the dominant partial melt product of Neoarchaean asthenosphere. If this is the case, then the Neoarchaean asthenosphere was not as refractory as the present-day and would therefore be a less suitable source for the generation of low-Ti rocks such as boninite.

In concluding the present contribution, we propose that the geochemical and Nd isotopic data presented here, in conjunction with the corresponding geochronological data (Davis et al., 2004) constitute the primary evidence that lithospheric processes similar to those responsible for the Eocene infant arc stages of the SW Pacific Ocean may have operated during the early stages of development of the CHSB.

Acknowledgments

Chris Hemmingway, Norah Brown, Thomas Hadlari and Yannick Beaudoin are warmly thanked for assistance in sample collection. Polar Continental Shelf Project supplied helicopter logistical support in the field. R. Thériault and K. Sankowski assisted in the acquisition of Nd isotopic data. The staff of the Geochemical Laboratories at the Geological Survey of Canada, McGill University, and of the Department of Earth Sciences at Memorial University of Newfoundland are thanked for the whole-rock analyses. Neil Rogers provided a thorough review of an earlier version of the manuscript. This is a contribution to the Western Churchill NATMAP Project, is Geological Survey of Canada contribution #2002284 and Polar Continental Shelf Project contribution #01404.

Appendix A. Analytical methods

Approximately 1 kg of each rock sample was crushed to chips in a Braun jaw crusher, and a 50 g split of each mafic rock was pulverized to a fine powder in an agate ring mill. Felsic rocks were pulverized in a tungsten carbide mill. Most analyses were obtained at the Geochemical Laboratories of the Geological Survey of Canada (Ottawa). Major elements and Ba were analyzed by X-Ray fluorescence analysis (XRF) of fused discs. Volatile contents, expressed as loss on ignition (LOI) were determined gravimetrically. The trace elements Ba, Co, Cr, Cu, Ni, Sc, V and Zn were analyzed by ICP-ES, whereas all other trace elements including Cs, Ga, Pb, Rb, Hf, Th, U, Ta, Nb, Y and the rare earth elements (REE) were determined through ICP-MS analysis. Analytical errors for the data, as based on the analysis of duplicates and of reference materials are calculated at <5% relative percent for the major elements, <10% for those trace elements determined by XRF, <10% for ICP-ES analyses<5% for ICP-MS analyses. These were supplemented by pressed powder disc, XRF analysis for the trace elements Zr, Nb and Ga (Department of Earth and Planetary Sciences, McGill University).

Analysis of selected rock samples were undertaken at the Department of Earth Sciences, Memorial University of Newfoundland. Major elements and the trace elements Cr, Ni, Sc, V, Cu, Zn and Zr were determined through XRF analysis of glass discs. LOI was obtained gravimetrically. All other elements were obtained through ICP-MS analysis following the method of Longerich et al. (1990).

Sm–Nd analyses were conducted at the Geochronological Laboratories of the Geological Survey of Canada (Ottawa) and analytical procedures are a variant of those documented by Thériault (1990). Whole-rock powders (ca. 0.2 g) were spiked with a $^{148}Nd/^{149}Nd$ mixed solution and dissolved in a warm $HF–HNO_3$ solution. Nd and Sm were separated using wet chemical chromatographic methods, ultra-pure acids and conventional cation specific separation resins. Isotopic ratios were determined by Thermal Ion Mass Spectrometry using a Finnigan Mat 261 solid source mass spectrometer run in the static mode. Neodymium isotopic compositions were normalized to $^{146}Nd/^{144}Nd = 0.7219$ and corrected to La Jolla $^{143}Nd/^{144}Nd = 0.511860$. Repeated analysis of an AMES standard Nd metal solution yielded $^{143}Nd/^{144}Nd = 0.512165 \pm 0.20$ (2σ). ϵNd values (DePaolo, 1981) were calculated using a present-day CHUR (chondritic uniform reservoir) composition of $^{143}Nd/^{144}Nd = 0.512638$ and $^{147}Sm/^{144}Nd = 0.1967$ (Jacobsen and Wasserburg, 1980). The reproducibility of the as ϵNd values are calculated to be ca. $\pm 0.5\epsilon$ units, whereas the reproducibility of the $^{147}Sm/^{144}Nd$ ratios is approximated at ca. 0.3%. Nd isotopic data for 23 samples are presented in Table 4.

References

Aspler, L.B., Chiarenzelli, J.R., 1996. Stratigraphy, sedimentology and physical volcanology of the Henik Group, central Ennadai–Rankin greenstone belt, Northwest Territories, Canada: Late Archean paleogeography of the Hearne Province and tectonic implications. Precambrian Res. 77, 59–89.

Barrie, C.T., Ludden, J.N., Green, T.H., 1993. Geochemistry of volcanic rocks associated with Cu–Zn and Ni–Cu deposits in the Abitibi subprovince. Econ. Geol. 88, 1341–1358.

Bloomer, S.H., Taylor, B., MacLeod, C.J., Stern, R.J., Fryer, P., Hawkins, J.W., Johnson, L., 1995. Early arc volcanism and the ophiolite problem: a perspective from drilling in the western Pacific. In active margins and marginal basins of the western Pacific, geophysics monograph. Amer. Geophys. Union 88.

Cas, R.A.F., Wright, J.V., 1987. Volcanic Successions. Allen and Unwin, London.

Cousens, B.L., 2000. Geochemistry of the Archean Kam Group, Yellowknife Greenstone Belt, Slave Province. Can. J. Geol. 108, 181–197.

Cousens, B.L., Aspler, L.B., Chiarenzelli, J.R., in press. Geochemistry and Sm–Nd isotopic compositions of Neoarchaean supracrustal and plutonic rocks, Henik segment, central Hearne sub-domain, Nunavut, Canada. Precambrian Res.

Davidson, A., 1970. Precambrian geology, Kaminak Lake map-area, District of Keewatin. Geol. Surv. Can. Pap. 69/51, 27.

Davis, W.J., Peterson, T.D., 1998. New geochronological results for the Tavani area (55K), eastern Kaminak greenstone belt, District of Keewatin, Northwest Territories. Geol. Surv. Can. Pap. 1998-F, 81–88.

Davis, W., Hanmer, S., Aspler, L., Sandeman, H., Tella, S., Zaleski, E., Relf, C., Ryan, J., Berman, R., MacLachlan, K., 2000. Regional differences in the Neoarchean crustal evolution of the Western Churchill Province: can we make sense of it? GeoCanada 2000. Geol. Ass. Can.—Min. Ass. Can. Joint Annual Meeting, Calgary, CDROM format.

Davis, W., Hanmer, S., Sandeman, H.A., 2004. Temporal evolution of the Neoarchaean Central Hearne supracrustal belt: rapid generation of juvenile crust in a suprasubduction zone setting. Precambrian Res. 134, 85–112.

DePaolo, D.J., 1981. Neodymium isotopes in the Colorado Front Range and crust–mantle evolution in the Proterozoic. Nature 291, 193–196.

Dostal, J., Mueller, W.U., 1997. Komatiite flooding of a rifted archean rhyolitic arc complex: geochemical signature and tectonic significance of the Stoughton–Roquemaure Group, Abitibi greenstone belt. Can. J. Geol. 105, 545–563.

Drummond, M.S., Defant, M.J., 1990. A model for trondhjemite–tonalite–dacite genesis and crustal growth via slab melting: Archean to modern comparisons. J. Geophys. Res. 95, 21503–21521.

Drummond, M.S., Defant, M.J., Kepezhinskas, P.K., 1996. Petrogenesis of slab-derived trondhjemite–tonalite–dacite/adakite magmas. Trans. Royal Soc. Edinburgh. 87, 205–215.

Elliott, T., Plank, T., Zindler, A., White, W., Bourdon, B., 1997. Element transport from slab to volcanic front at the Mariana arc. J. Geophys. Res. 102, 14991–15019.

Francis, D., 2003. Cratonic mantle roots, remnants of a more chondritic Archean mantle? Lithos 71, 135–152.

Fretzdorff, S., Livermore, R.A., Devey, C.W., Leat, P.T., Stoffers, P., 2002. Petrogenesis of the bacK–Arc East Scotia Ridge, South Atlantic Ocean. J. Petrol. 43, 1435–1467.

Gribble, R.F., Stern, R.J., Newman, S., Bloomer, S.H., O'Hearn, T., 1998. Chemical and isotopic composition of lavas from the northern Mariana trough: implications for magma genesis in bacK–Arc basins. J. Petrol. 39, 125–154.

Hanmer, S., Sandeman, H.A., Davis, W.J., Aspler, L.B., Rainbird, R.H., Peterson, T.D., Ryan, J.J., Roest, W.R., Relf, C., Irwin, D., in press. Tectonic setting of the Neoarchaean Henik–Kaminak–Tavani supracrustal belt, Western Churchill province, Canada: a geological perspective. Precambrian Res.

Hanmer, S., Relf, C., 2000. Western Churchill NATMAP Project: new results and potential significance. GeoCanada 2000. Geol. Ass. Can.—Min. Ass. Can. Joint Annual Meeting, Calgary, CDROM format.

Hawkins, J.W., 1995. Evolution of the Lau Basin—insights from ODP Leg 135. In Active Margins and Marginal Basins of the Western Pacific, Geophysics Monograph 88, Amer. Geophys. Union.

Hollings, P., 2002. Archean Nb-enriched basalts in the northern Superior Province. Lithos 64, 1–14.

Hollings, P., Kerrich, R., 2000. An Archean arc basalt ± Nb-enriched basalt ± adakite association: the 2.7 Ga confederation assemblage of the Birch ± Uchi greenstone belt, Superior Province. Contrib. Mineral. Petrol. 139, 208–226.

Hollings, P., Wyman, D., Kerrich, R., 1999. Komatiite–basalt–rhyolite volcanic associations in Northern Superior Province greenstone belts: significance of plume-arc interaction in the generation of proto continental Superior Province. Lithos 46, 137–161.

Hoffman, P.F., 1988. United Plates of America, the birth of a craton: early Proterozoic assembly and growth of Laurentia. Ann. Rev. Earth Planet Sci. 16, 543–603.

Irvine, T.N., Barager, W.R.A., 1971. A guide to the chemical classification of the common volcanic rocks. Can. J. Earth Sci. 8, 523–548.

Jacobsen, S.B., Wasserburg, G.J., 1980. Sm–Nd isotopic evolution of chondrites. Earth Planet Sci. Lett. 50, 139–155.

Kamber, B.S., Ewart, A., Collerson, K.D., Bruce, M.C., McDonald, G.D., 2002. Fluid-mobile trace element constraints on the role of slab melting and implications for Archaean crustal growth models. Contrib. Mineral. Petrol. 144, 38–56.

Kerrich, R., Wyman, D., Fan, J., Bleeker, W., 1998. Boninite series: low Ti–tholeiite associations from the 2.7 Ga Abitibi greenstone belt. Earth Planet Sci. Lett. 164, 303–316.

Lafleche, M.R., Dupuy, C., Dostal, J., 1992. Tholeiitic volcanic rocks of the Late Archean Blake River Group, Southern Abitibi greenstone belt: origin and geodynamic implications. Can. J. Earth Sci. 29, 1448–1458.

LeBas, M.J., LeMaitre, R.W., Streckeisen, A., Zanettin, B., 1986. A chemical classification of volcanic rocks based on the total alkali silica diagram. J. Petrol. 27, 745–750.

Lesher, C.M., Goodwin, A.M., Campbell, I.H., Gorton, M.P., 1986. Trace-element geochemistry of ore-associated and barren, felsic metavolcanic rocks in the Superior Province. Can. J. Earth Sci. 23, 222–237.

Longerich, H.P., Jenner, G.A., Fryer, B.J., Jackson, S.E., 1990. Inductively coupled plasma-mass spectrometric analysis of geologic samples: a critical evaluation based on case studies. Chem. Geol. 83, 105–118.

Martin, H., 1987. Petrogenesis of Archean trondhjemites, tonalites, and granodiorites from eastern Finland: major and trace element geochemistry. J. Petrol. 28, 921–953.

Martin, H., 1999. Adakitic magmas: modern analogues of Archaean granitoids. Lithos 46, 411–429.

Middelburg, J.J., Van der Weijden, C.H., Woittiez, J.R.W., 1988. Chemical processes affecting the mobility of major, minor and trace elements during weathering of granitic rocks. Chem. Geol. 68, 253–273.

Miller, A., Tella, S., 1995. Stratigraphic setting of semi-conformable alteration in the Spi Lake area, Kaminak greenstone belt, Churchill Province, Northwest Territories. Geol. Surv. Can. Pap. 1995-c, 175–186.

Miyashiro, A., 1974. Volcanic rock series in island arcs and active continental margins. Am. J. Sci. 274, 321–355.

Mortensen, J.K., Thorpe, R.I., 1987. U–Pb zircon ages of felsic volcanic rocks in the Kaminak Lake area, District of Keewatin. Geol. Surv. Can. Pap. 87/2, 123–128.

Mueller, W., Chown, E.H., Sharma, K.N.M., Tait, L., Rocheleau, M., 1989. Paleogeographic and paleotectonic evolution of a basement-controlled Archean supracrustal sequence, Chibougamau. Quebec J. Geol. 97, 399–420.

Ohta, H., Maruyama, S., Takahashi, E., Watanabe, Y., Kato, Y., 1996. Field occurrence, geochemistry and petrogenesis of the Archean Mid-Oceanic Ridge Basalts (AMORBs) of the Cleaverville area, Pilbara Craton, Western Australia. Lithos 37, 199–221.

Park, A.F., Ralser, S., 1992. Precambrian Geology of the southwestern part of the Tavani map area, District of Keewatin, Northwest Territories. Geol. Surv. Can. Bull. 416, 81.

Patterson, J.G., Heaman, L.M., 1990. Geochronological constraints on the depositional age of the Hurwitz Group, N.W.T. Geol. Ass. Can. Prog. Abstr. 15, A102.

Pearce, J.A., 1982. Trace element characteristics of lavas from destructive plate boundaries. In: Thorpe, R.S. (Ed.), Andesites, John Wiley and Sons, pp. 525–548.

Pearce, J.A., 1996. A user's guide to basalt discrimination diagrams. In: Trace element geochemistry of volcanic rocks; applications

for massive sulphide exploration. Short course notes. Geol. Ass. Can. 12, 79–113.

Pearce, J.A., Cann, J.R., 1973. Tectonic setting of basic volcanic rocks determined using trace element analyses. Earth Planet Sci. Lett. 19, 290–300.

Pearce, J.A., Norry, M.J., 1979. Petrogenetic implications of Ti, Zr, Y and Nb variations in volcanic rocks. Contrib. Mineral. Petrol. 69, 33–47.

Pearce, J.A., and Peate, D.W., 1995. Tectonic implications of the composition of volcanic arc magmas. In: Wetherill, G.W., Albee, A.L., Burke, K.C. (Eds.), Ann. Rev. Earth Plan. Sci. 23, pp. 251–285.

Pearce, J.A., Lippard, S.J., Roberts, S., 1984. Characteristics and tectonic significance of supra-subduction zone ophiolites. In: Kokelaar, B.P., Howells, M.F. (Eds.), Geol. Soc. Spec. Pub. Blackwell Scientific, London, pp. 77–94.

Pearce, J.A., Ernewein, M., Bloomer, S.H., Parson, L.M., Murton, B.J., Johnson, L.E. 1995. Geochemistry of Lau Basin volcanic rocks: influence of ridge segmentation and arc proximity. In: Smellie, J.L. (Ed.), Volcanism Associated with Extension at Consuming Plate Margins. Geol. Soc. Spec. Pub. 81, pp. 53–75.

Polat, A., Kerrich, R., Wyman, D.A., 1998. The late Archean Schreiber–Hemlo and White River–Dayohessarah greenstone belts, Superior Province: collages of oceanic plateaus, oceanic arcs, and subduction–accretion complexes. Tectonophysics 289, 295–326.

Rainbird, R.H., Hadlari, T. 1998. Intra-arc sedimentation in the Neoarchean Kaminak Group, Quartzite Lake area, Kivalliq Region (abstract) 25th Yellowknife Geoscience Forum, Program and Abstracts of Talks and Posters, 26–28 November 1998.

Ridler, R.H., 1973. Volcanic stratigraphy and metallogeny; Rankin Inlet-Ennadai belt, District of Keewatin. Geol. Surv. Can. Pap. 73-1A, 165–174.

Roeder, P.L., Emslie, R.F., 1970. Olivine–liquid equilibrium. Contrib. Mineral. Petrol. 29, 275–289.

Rollinson, H.R., 1993. Using Geochemical Data: Evaluation, Presentation and Interpretation. Longman Scientific and Technical Press, Harlow, UK.

Sajona, F.G., Maury, R.C., Bellon, H., Cotton, J., Defant, M., 1996. High field strength element enrichment of Pliocene–Pleistocene island arc basalts, Zamboanga Peninsula, Western Mindanao (Philippines). J. Petrol. 37, 693–726.

Sandeman, H.A.I., 1995. Lithostratigraphy, petrology and geochronology of the Crucero Supergroup, Puno, SE Peru: implications for the Cenozoic geodynamic evolution of the southern Peruvian Andes. Unpublished Ph.D. thesis, Queen's University, 381p.

Sandeman, H.A., Davis, W., Hanmer, S., MacLachlan, K., Ryan, J., Kjarsgaard, B., Kerswill, J., Tella, S., Zaleski, E., Cousens, B., Relf, C. 2000. Archean volcanic sequences of the Western Churchill Province, Nunavut, Canada: three petrochemically distinct domains of non-plateau affinity. GeoCanada 2000. Geol. Ass. Can.—Min. Ass. Can. Joint Annual Meeting, Calgary, CDROM format.

Sandeman, H.A., Hanmer, S., Davis, W., 2001. Archean supracrustal belts, Hearne domain, Canada: a proto-arc/bacK–Arc pair? (extended abstract) Fourth International Archean Symposium, September 2001, Perth, Australia.

Sandeman, H.A., Davis, W.J., Peterson, T.D., Hanmer, S., Ryan, J.J., 2004. Whole-rock and Nd isotopic geochemistry of Neoarchaean granitoids and their bearing on the evolution of the Central Hearne supracrustal belt, Western Churchill Province. Canada. Precambrian Res. 134, 143–167.

Saunders, A.D., Tarney, J., 1991. BacK–Arc basins. In: Floyd, P.-A. (Ed.), Oceanic basalts. Blackie and Son, Glasgow, UK, pp. 219–263.

Smithies, R.H., 2000. The Archaean tonalite–trondhjemite–granodiorite (TTG) series is not an analogue of Cenozoic adakite. Earth Planet Sci. Lett. 182, 115–125.

Stern, R.A., Syme, E.C., Bailes, A.H., Lucas, S.B., 1995. Paleoproterozoic (1.90–1.86 Ga) arc volcanism in the Flin Flon Belt, Trans-Hudson Orogen. Can. Contrib. Mineral. Petrol. 119, 117–141.

Stern, R.A., Berman, R.G., 2000. Monazite U–Pb and Th–Pb geochronology by ion microprobe, with an application to in situ dating of an Archean metasedimentary rock. Chem. Geol. 172, 113–130.

Stern, R.J., Bloomer, S.H., 1992. Subduction zone infancy: examples from the Izu–Bonin–Mariana and Jurassic California arcs. Geol. Soc. Am. Bull. 104, 1621–1636.

Stockwell, C.H., 1982. Proposals for time classification and correlation of Precambrian rocks and events in Canada and adjacent areas of the Canadian Shield. Part 1: a time classification of precambrian rocks and events. Geol. Surv. Can. Spec. Pap., 19–80.

Sun, S.-S., McDonough, W.F., 1989. Chemical and isotopic systematics of oceanic basalts: implications for mantle composition and processes. In: Saunders, A.D., Norry, M.J. (Eds.), Magmatism in the Ocean Basins, 42. Geol. Soc. Spec. Pub, pp. 313–345.

Thériault, R.J., 1990. Methods for Rb–Sr and Sm–Nd isotopic analyses at the geochronology laboratory. Geological Survey of Canada. Geol. Surv. Can. Pap. 1989-2, 3–6.

Thériault, R.J., Tella, S., 1997. Sm–Nd isotopic study on mafic volcanic rocks from the Rankin Inlet and Tavani regions, District of Keewatin, Northwest Territories. Geol. Surv. Can. Pap. 1997-F, 61–66.

Tomlinson, K.Y., Condie, K., 2001. Archean mantle plumes: evidence from greenstone belt geochemistry. Geol. Soc. Am. Spec. Pap. 352, 341–357.

Tomlinson, K.Y., Stevenson, R.K., Hughes, D.J., Hall, R.P., Thurston, P.C., Henry, P., 1998. The Red Lake greenstone belt, Superior Province: evidence of plume-related magmatism at 3 Ga and evidence of an older enriched source. Precambrian Res. 89, 59–76.

Tomlinson, K.Y., Hughes, D.J., Thurston, P.C., Hall, R.P., 1999. Plume magmatism and crustal growth at 2.9 to 3.0 Ga in the Steep Rock and Lumby Lake area, Western Superior Province. Lithos 46, 103–136.

Tomlinson, K.Y., Davis, D.W., Percival, J.A., Hughes, D.J., Thurston, P.C., 2002. Mafic to felsic magmatism and crustal recycling in the Obonga Lake greenstone belt, western Superior Province: evidence from geochemistry, Nd isotopes and U–Pb geochronology. Precambrian Res. 114, 295–325.

Winchester, J.A., Floyd, P.A., 1977. Geochemical discrimination of different magma series and their differentiation products using immobile elements. Chem. Geol. 20, 325–343.

Wolde, B., Asres, Z., Desta, Z., Gonzalez, J.J., 1996. Neoproterozoic zirconium-depleted boninite and tholeiitic series rocks from Adola, southern Ethiopia. Precambrian Res. 80, 261–279.

Wood, D.A., Joron, J.L., Treuil, M., 1979. A re-appraisal of the use of trace elements to classify and discriminate between magma series erupted in different tectonic settings. Earth Planet Sci. Lett. 50, 326–336.

Wyman, D.A., Bleeker, W., Kerrich, R., 1999. A 2.7 Ga komatiite, low Ti tholeiite, arc tholeiite transition, and inferred proto-arc geodynamic setting of the Kidd Creek deposit: evidence from precise trace element data. Econ. Geol. Monograph 10, 511–528.

Wyman, D.A., Ayer, J., Devaney, J., 2000. Niobium-enriched basalts from the Wabigoon subprovince, Canada: evidence for adakitic metasomatism above an Archean subduction zone. Earth Planet Sci. Lett. 179, 21–30.

Wyman, D.A., Kerrich, R., Polat, A., 2002. Assembly of Archean cratonic mantle lithosphere and crust: plume-arc interaction in the Abitibi–Wawa subduction–accretion complex. Precambrian Res. 115, 37–62.